Moreover, apoptosis was increased in the heart of tissue-specific Tfam knockouts (Wang *et al.*, 2001). Additionally, mice expressing a proofreading-deficient version of mitochondrial DNA polymerase γ accumulated mtDNA mutations, and the levels of the accumulated mutations correlated with the induction of apoptotic markers (Kujoth *et al.*, 2005; Trifunovic *et al.*, 2005). These data provide *in vivo* evidence that the respiratory chain deficiency predisposes cells to apoptosis.

Development of tolerance to apoptosis by mutant mitochondrial DNA

An immortalized human fibroblast cell line carrying wild-type mtDNA underwent apoptosis in a high concentration of molecular oxygen. In contrast, its $\rho 0$ exhibited a marked resistance to apoptosis (Yoneda *et al.*, 1995). Additionally, $\rho 0$ cells showed a stronger resistance to irradiation than the other two cell lines (Tang *et al.*, 1999). $\rho 0$ cells were more resistant to apoptosis-inducing agents than parental cells *in vitro* (Singh *et al.*, 1999; Wang *et al.*, 2001). In these experiments, parental cells or the other cell lines were used as controls. One should bear in mind that it is highly possible to introduce considerable mutations into nuclear genes of $\rho 0$ cells by long exposure to EtBr during the isolation of a $\rho 0$ cell line. Nevertheless, these consistent results obtained from various lines of research suggest that they may be negligible.

As mentioned above, *in vivo* $\rho 0$ or mtDNA-mutant cells are more sensitive to apoptosis, while $\rho 0$ cells in culture are more resistant to various apoptotic stimuli. This discrepancy may be explained as follows: cultured $\rho 0$ cells may adapt to cope with the bioenergetic crisis conditions perhaps because by enhancing the activity of the glycolytic pathway. However, *in vivo* cells cannot adapt in response to a transient depletion. The process of malignant transformation usually takes a long time. Thus, cancer cells selected during this process are likely better adapted to cope with the energetic demands. Since cybrid cells were derived from $\rho 0$ cells, they should also be fully adapted. Thus, mtDNA-mutant cybrids are more resistant to apoptosis induced by various stimuli. It remains unclear why $\rho 0$ and mtDNA-mutant cybrid cells are more resistant to induction of apoptosis at the molecular level.

To understand the molecular mechanism underlying the association between decline of an energy production and sensitivity to apoptosis, it is important to know the expression profiles of nuclear genes. Transient depletion of mtDNA or treatment with mitochondrial poison CCCP initiates mitochondrial stress signaling, which operates through altered Ca^{2+} homeostasis. In myoblasts and human lung carcinoma cells, mitochondrial stress signaling activates calcineurin and a number of Ca^{2+}-responsive factors including activating transcription factor, nuclear factor of activated T cells, CCAAT enhancer-binding protein/δ and cAMP-responsive element binding protein. Additionally, protein kinase C and mitogen-activated protein kinase are also activated. Nuclear gene targets including those involved in Ca^{2+} storage/release, glucose metabolism, oncogenesis and apoptosis are upregulated. Mitochondrial stress in both the myoblasts and lung carcinoma cells induced morphological changes and invasive phenotypes (Biswas *et al.*, 2005). It is important to investigate the molecular mechanism underlying tolerance to apoptosis from the aspects of nuclear gene expression and regulation.

Mitochondrial DNA mutations confer tolerance to anticancer drugs

Emergence of drug resistance is a critical problem for chemotherapy, but the mechanisms underlying this phenomenon are not completely understood. Most anticancer drugs are inducers of apoptosis. As mentioned above, mutant mtDNA in cybrids confer resistance to apoptosis. When cybrids were treated with cisplatin, a typical anticancer drug, mutant cybrids were more resistant to apoptosis than the wild-type (Shidara *et al.*, 2005).

Another report supports our results that mutant cybrids are more resistant to anticancer drugs. $\rho 0$ cells are extremely resistant to adriamycin and photodynamic therapy (Singh *et al.*, 1999) and cisplatin (Qian *et al.*, 2005). Tolerance to etoposide was found even by the transient depletion of mtDNA (Biswas *et al.*, 2005).

Interestingly, ATP synthase is downregulated in some 5-fluorouridine (5-FU)-resistant cells, which also showed decreased ATP synthase activity and reduced

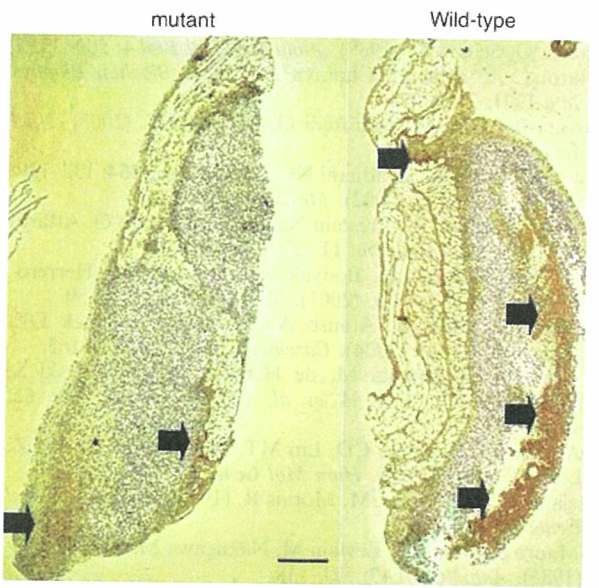

Figure 5 Tolerance to cisplatin in tumors derived from cybrids possessing mutant mitochondrial DNA (mtDNA). Cybrids carrying mtDNA with a homoplasmic mutation in the cytochrome *c* oxidase subunit I gene were transplanted into nude mice. Cisplatin was administrated to the nude mice and the tumors were evaluated for apoptosis by the terminal deoxy transferase uridine triphosphate nick end labeling (TUNEL) method. Arrows indicate massive TUNEL-positive areas. Right panel indicates a tumor derived from wild-type cybrids, while the left panel from mutant cybrids. Scale bar: 0.5 mm.

intracellular ATP content (Shin *et al.*, 2005). When 5-FU sensitivity was compared with ATP synthase activity in six different human colon cancer cell lines, positive correlation was observed. The bioenergetic dysfunction of mitochondria has been reported as a hallmark of many types of cancers; that is, downregulation of ATP synthase β-subunit expression in liver, kidney, colon, squamous esophageal, and lung carcinomas, as well as in breast and gastric adenocarcinomas (Cuezva *et al.*, 2002, 2004; Isidoro *et al.*, 2004). Thus, decreased ATP synthase activity may be associated with resistance to some anticancer drugs. Tolerance to anticancer drugs is due not only to the decline of ATP synthase activity, but rather to alterations in mitochondrial activity. We constructed cybrids harboring mutant mtDNA derived from pancreatic cancer cells. Mutant mtDNA have a mutation at cytochrome *c* oxidase or the subunit 4 of complex I (ND4). The cybrids were strongly resistant to cisplatin and 5-FU *in vivo* and *in vitro* (Figure 5) (manuscript in preparation).

Mitochondria are directly involved in apoptosis by releasing factors involved in the initiation, regulation and execution of apotosis (Ohta, 2003). Members of the bcl-2 family regulate apoptosis on mitochondria. To understand the link between mitochondrial dysfunction and apoptosis at the molecular level, the response profiles of these factors to mitochondrial dysfunction will be investigated. Alternatively, it seems important to highlight cross-talk between the nucleus and mitochondria. The expression of apoptosis regulators may be influenced by dysfunctional mitochondrial through a decrease in ATP, a Ca^{2+} signaling or an increase in lactate or pyruvate by enhancing glycolysis.

Concluding remarks

Methods that had been developed to clarify the responsibility of mutant mtDNA in mitochondrial diseases were applied to investigate its role in tumorigenesis. Cybrids containing a common nucleus and mtDNA with a pathogenic mutation revealed an apparent advantage in growth when transplantated into nude mice. This advantage is related to alterations in mitochondrial activity, but not secondary mutations in the nuclear genome. However, tumors formed by cybrid transplantation may differ in many ways from naturally occurring cancers. More careful investigation will be required to understand the veritable roles of mtDNA in cancer. Additionally, we addressed the role of mutant mtDNA in conferring tolerance to anticancer drugs. By understanding the molecular mechanism of how to gain tolerance, mtDNA will be extensively investigated for clinical application in the light of apoptosis.

References

Amuthan G, Biswas G, Zyang SY, Klein-Szanto A, Vijayasarathy C, Avadhani NG. (2001). *EMBO J* **20**: 1910–1920.
Attardi G, Schatz G. (1988). *Annu Rev Cell Biol* **4**: 289–333.
Attardi G, Yoneda M, Chomyn A. (1995). *Biochim Biophys Acta* **1271**: 241–248.
Bayona-Bafaluy MP, Manfredi G, Moraes CT. (2003). *Nucl Acids Res* **31**: e98.
Biswas G, Guha M, Avadhani NG. (2005). *Gene* **354**: 132–139.
Carew JS, Huang P. (2002). *Mol Cancer* **1**: 9.
Chomyn A, Meola G, Bresolin N, Lai ST, Scarlato G, Attardi G. (1991). *Mol Cell Biol* **11**: 2236–2244.
Coller HA, Khrapko K, Bodyak ND, Nekhaeva E, Herrero-jimenez P, Thilly WG. (2001). *Nat Genet* **28**: 147–150.
Cuezva JM, Chen G, Alonso AM, Isidoro A, Misek DE, Hanash SM *et al.* (2004). *Carcinogenesis* **25**: 1157–1163.
Cuezva JM, Krajewska M, de Heredia ML, Krajewski S, Santamaria G, Kim H *et al.* (2002). *Cancer Res* **62**: 6674–6681.
D'Aurelio M, Gajewski CD, Lin MT, Mauck WM, Shao LZ, Lenaz G *et al.* (2004). *Hum Mol Genet* **13**: 3171–3179.
Desjardins P, de Muys JM, Morais R. (1986). *Somat Cell Mol Genet* **12**: 133–139.
DiMauro S, Bonilla E, Zeviani M, Nakagawa M, DeVivo DC. (1985). *Ann Neurol* **17**: 521–538.
Dunbar DR, Moonie PA, Jacobs HT, Holt IJ. (1995). *Proc Natl Acad Sci USA* **92**: 6562–6566.
Evans AR, Limp-Foster M, Kelley MR. (2000). *Mutat Res* **461**: 83–108.
Fliss MS, Usadel H, Caballero OL, Wu L, Buta MR, Eleff SM *et al.* (2000). *Science* **287**: 2017–2019.
Geromel V, Kadhom N, Cebalos-Picot I, Ouari O, Polidori A, Munnich A *et al.* (2001). *Hum Mol Genet* **10**: 1221–1228.
Ghelli A, Zanna C, Porcelli AM, Schapira AH, Martinuzzi A, Carelli V *et al.* (2003). *J Biol Chem* **278**: 4145–4150.
Guy J, Qi X, Pallotti F, Schon EA, Manfredi G, Carelli V *et al.* (2002). *Ann Neurol* **52**: 534–542.
Hayashi J, Ohta S, Kikuchi A, Takemitsu M, Goto Y, Nonaka I. (1991a). *Proc Natl Acad Sci USA* **88**: 10614–10618.
Hayashi J, Ohta S, Takai D, Miyabayashi S, Sakuta R, Goto Y *et al.* (1993). *Biochem Biophys Res Commun* **197**: 1049–1055.
Hayashi J, Tanaka M, Sato W, Ozawa T, Yonekawa H, Kagawa Y *et al.* (1990). *Biochem Biophys Res Commun* **167**: 216–221.
Hayashi J, Yonekawa H, Watanabe S, Nonaka I, Momoi M, Kagawa Y *et al.* (1991b). Somatic cell genetical approaches to mitochondrial diseases. In: Sato T, DiMauro S (eds). *Progress in Neuro-pathology*. Raven: New York, pp 93–102.
Hayashi JI, Takemitu M, Nonaka M. (1992). *Somatic Cell Mol Genet* **18**: 123–129.
Holt IJ, Harding AE, Petty RK, Morgan-Hughes JA. (1990). *Am J Hum Genet* **46**: 428–433.
Inoue K, Ito S, Takai D, Soejima A, Shisa H, LePecq JB *et al.* (1997). *J Biol Chem* **272**: 15510–15515.
Isidoro A, Martinez M, Fernandez PL, Ortega AD, Santamaria G, Chamorro M *et al.* (2004). *Biochem J* **378**: 17–20.
King MP, Attardi G. (1989). *Science* **246**: 500–503.
King MP, Koga Y, Davidson M, Schon EA. (1992). *Mol Cell Biol* **12**: 480–490.
Klein TM, Fitzpatrick-McElligott S. (1993). *Curr Opin Biotechnol* **4**: 583–590.
Kujoth GC, Hiona A, Pugh TD, Someya S, Panzer K, Wohlgemuth SE *et al.* (2005). *Science* **309**: 481–484.
Lee SR, Kwon KS, Kim SR, Rhee SG. (1998). *J Biol Chem* **273**: 15366–15372.
Lightowlers RN, Chinnery PF, Turnbull DM, Howell N. (1997). *Trends Genet* **13**: 450–455.

Linnartz B, Anglmayer R, Zanssen S. (2004). *Cancer Res* **64**: 1966–1971.
Liu VW, Shi HH, Cheung AN, Chiu PM, Leung TW, Nagley P *et al.* (2001). *Cancer Res* **61**: 5998–6001.
Manfredi G, Fu J, Ojaimi J, Sadlock JE, Kwong JQ, Guy J *et al.* (2002). *Nat Genet* **30**: 394–399.
Matsuzawa A, Saegusa K, Noguchi T, Sadamitsu C, Nishitoh H, Nagai S *et al.* (2005). *Nat Immunol* **6**: 587–592.
Maximo V, Soares P, Lima J, Cameselle-Teijeiro J, Sobrinho-Simoes M. (2002). *Am J Pathol* **160**: 1857–1865.
McCord JM. (2000). *Am J Med* **108**: 652–659.
Michiels C, Minet E, Mottet D, Raes M. (2002). *Free Radic Biol Med* **33**: 1231–1242.
Moraes CT, Dey R, Barrientos A. (2001). *Methods Cell Biol* **65**: 397–412.
Morais R, Zinkewich-Peotti K, Parent M, Wang H, Babai F, Zollinger M. (1994). *Cancer Res* **54**: 3889–3896.
Nakano K, Ohsawa I, Yamagata K, Nakayama T, Sasaki K, Tarashima M *et al.* (2003). *Mitochondrion* **3**: 21–27.
Nakashima-Kamimura N, Asoh S, Ishibashi Y, Mukai Y, Shidara Y, Oda H *et al.* (2005). *J Cell Sci* **118**: 5357–5367.
Nishikawa M, Nishiguchi S, Shiomi S, Tamori A, Koh N, Takeda T *et al.* (2001). *Cancer Res* **61**: 1843–1845.
Ohta S. (2003). *Curr Med Chem* **10**: 2485–2494.
Parrella P, Xiao Y, Fliss M, Sanchez-Cespedes M, Mazzarelli P, Rinaldi M *et al.* (2001). *Cancer Res* **61**: 7623–7626.
Petros JA, Baumann AK, Ruiz-Pesini E, Amin MB, Sun CQ, Hall J *et al.* (2005). *Proc Natl Acad Sci USA* **102**: 719–724.
Polyak K, Li Y, Zhu H, Lengauer C, Willson JK, Markowitz SD *et al.* (1998). *Nat Genet* **20**: 291–293.
Qian W, Nishikawa M, Haque AM, Hirose M, Mashimo M, Sato E *et al.* (2005). *Am J Physiol Cell Physiol* **289**: 1466–1475.
Shidara Y, Yamagata K, Kanamori T, Nakano K, Kwong JQ, Manfredi G *et al.* (2005). *Cancer Res* **65**: 1655–1663.
Shin YK, Yoo BC, Chang HJ, Jeon E, Hong SH, Jung MS *et al.* (2005). *Cancer Res* **65**: 3162–3170.
Singh KK, Russell J, Sigara B, Zhang T, Williams J, Keshav KF. (1999). *Oncogene* **18**: 6641–6646.
Takamatsu C, Umeda S, Ohsato T, Ohno T, Abe Y, Fukuoh A *et al.* (2002). *EMBO J* **3**: 451–456.
Tan DJ, Bai RK, Wong LJ. (2002). *Cancer Res* **62**: 972–976.
Tang JT, Yamazaki H, Inoue T, Koizumi M, Yoshida K, Ozeki S *et al.* (1999). *Anticancer Res* **19**: 4959–4964.
Tatuch Y, Christodoulou J, Feigenbaum A, Clarke JT, Wherret J, Smith C *et al.* (1992). *Am J Hum Genet* **50**: 852–858.
Trifunovic A, Hansson A, Wredenberg A, Rovio AT, Dufour E, Khvorostov I *et al.* (2005). *Proc Natl Acad Sci USA* **102**: 17993–17998.
Wang J, Silva JP, Gustafsson CM, Rustin P, Larsson NG. (2001). *Proc Natl Acad Sci USA* **98**: 4038–4043.
Warburg O. (1930). *The Metabolism of Tumors*. Constable Co. Ltd.: London.
Warburg O. (1956). *Science* **123**: 309–314.
Wong LJ, Lueth M, Li XN, Lau CC, Vogel H. (2003). *Cancer Res* **63**: 3866–3871.
Xu RH, Pelicano H, Zhou Y, Carew JS, Feng L, Bhalla KN *et al.* (2005). *Cancer Res* **15**: 613–621.
Yasukawa T, Yang MY, Jacobs HT, Holt IJ. (2005). *Mol Cell* **18**: 651–662.
Yeh JJ, Lunetta KL, van Orsouw NJ, Moore Jr FD, Mutter GL, Vijg J *et al.* (2000). *Oncogene* **19**: 2060–2066.
Yoneda M, Chomyn A, Martinuzzi A, Hurko O, Attardi G. (1992). *Proc Natl Acad Sci USA* **89**: 11164–11168.
Yoneda M, Katsumata K, Hayakawa M, Tanaka M, Ozawa T. (1995). *Biochem Biophys Res Commun* **209**: 723–729.

Journal of Neuro-Oncology (2005) 72: 231–238
DOI 10.1007/s11060-004-2353-3

Laboratory Investigation

Prognostic significance of the immunohistochemical index of survivin in glioma: a comparative study with the MIB-1 index

Masaki Uematsu[1,4], Ikuroh Ohsawa[1], Toshiyuki Aokage[1], Kiyomi Nishimaki[1], Kouji Matsumoto[2], Hiroshi Takahashi[3], Sadamitsu Asoh[1], Akira Teramoto[4] and Shigeo Ohta[1]
[1]*Department of Biochemistry and Cell Biology, Institute of Development and Aging Sciences, Graduate School of Medicine, Nippon Medical School, Kawasaki, Japan;* [2]*Departments of Pathology;* [3]*Neurosurgery, Second Hospital of Nippon Medical School, Kawasaki, Japan;* [4]*Department of Neurosurgery, Nippon Medical School, Tokyo, Japan*

Key words: glioma, MIB-1 index, prognosis, survivin, tumor marker

Summary

Objective: Survivin has been identified as a protein expressed in cancer cells and a member of the inhibitor-of-apoptosis protein family. Recent studies suggest that the expression of survivin increases during the G2/M phase of the cell cycle, and may be used in clinical prognosis. We examined whether survivin expression in human gliomas would be a correlative of prognosis.

Methods: We prepared polyclonal anti-survivin serum to establish a survivin index for stained sections, using an immunohistochemical procedure, according to the method used for scoring MIB-1 index, and then stained 29 paraffin-embedded sections from surgical specimens of 29 patients who were classified into three grades of World Health Organization with the mean age of low grade astocytoma (grade II) being 34.7; anaplastic astrocytoma (grade III), 48.8; and glioblastoma multiform (grade IV), 58.4.

Results: On staining with the anti-survivin antiserum, all specimens contained positive cells, but the survivin index was heterogeneous among grades. The mean percentage of immunoreactive cells in each specimen was 70.0% (SD 18.2%) in grade II, 81.3% (16.5%) in grade III, and 85.0% (13.6%) in grade IV. Then we compared the survivin index to the MIB-1 index and found that in low-grade gliomas (grade II and III), the difference in survival times between the high and low survivin indexes was significant ($P = 0.007$), whereas that between the high and low MIB-1 indexes was not significant ($P = 0.092$).

Conclusion: Survivin is more sensitive marker than MIB-1 for the evaluation of low-grade gliomas in that it helps to predict patient survival. Much larger glioma patient series are needed to validate the findings of our limited study.

Introduction

Glioma, the most common neoplasm in the human brain, includes tumors derived from astrocytes, oligodendrocytes, ependyma, and choroid plexus epithelium. Gliomas are histologically divided into four grades according to World Health Organization (WHO) guidelines. High grade glioma, GBM (glioblastoma multiform; grade IV), has the worst prognosis with a median survival time of about 12 months, even after surgical resection, radiation therapy, and chemotherapy. Of lower grade gliomas, patients with anaplastic astrocytoma (grade III) have an average survival of 3 years, whereas patients with low grade astrocytoma (grade II) have a better prognosis, with at least 5 years median survival [1]. However, the outcome for patients with anaplastic and low grade astrocytoma is highly variable [2,3]. A significant number of patients rapidly develop malignant glioma [4,5]. It has been reported that the proportion of tumor cells with abnormal p53 immunoreactivity increases in astrocytomas as they undergo malignant progression [6,7]. Thus, an accurate diagnosis is important from both clinical and experimental perspectives.

To date a number of methods for predicting the prognostic subgroups of glioma patients have been described [2,3]. One of the methods, the immunohistochemical determination of proliferative activity with the monoclonal antibody MIB-1 against Ki-67, which is a nuclear antigen, has been widely demonstrated to be clinically useful in distinguishing the biologic behavior of many tumors [5,8]. However, conflicting results from the utilization of Ki-67 as a prognostic marker for glioma especially for low grade glioma, have been reported [9–11].

Survivin is a member of the inhibitor-of-apoptosis protein (IAP) family and has been implicated in both the inhibition of apoptosis and regulation of mitosis [12,13]. IAPs are characterized by the presence of one to three baculovirus inhibitor apoptotic protein repeat domains, which often function as an inhibitor of the cell death process. The survivin gene is of the telomeric position on chromosome 17, to band q25 and its expression is determined in the developing embryo and in rapidly dividing cells including many human cancers [14,15]. Previous studies demonstrated that survivin is expressed at G2/M in a cell-cycle dependent manner and associated with kinetochores of metaphase chromosomes and

the central spindle midzone at anaphase, suggesting that survivin participates as a chromosomal passenger protein in cleavage furrow formation [13,16]. *In vitro*, it bound polymerized microtubles and a putative tubulin-binding domain was identified by mutational analysis. Forced expression of survivin counteracted cell death induced by various apoptotic stimuli, whereas interference with the expression or function of survivin by a dominant negative form or antisense of survivin caused spontaneous apoptosis and multiple cell division defects, suggesting that survivin acts both as a mitotic regulator and as a cytoprotective factor at cell division [16,17].

Overexpression of survivin has been observed in most human cancers including glioma by analysis of its mRNA and/or protein, whereas a low level of survivin expression is detected in normal tissues [18,19]. Recently, Chakravarti et al. has reported that the quantitative determination of survivin by Western blot analysis is useful for prognosis in human glioma [20]. However, in their study, survivin was not detected in 36% of gliomas. Thus, the aim of this study was to evaluate the histological determination of survivin with a sensitive anti-survivin anti-serum in a consecutive series of low- and high-grade gliomas to assess the prognostic significance of survivin expression. We here demonstrated that all gliomas expressed survivin and that the percentage of immunoreactive cells (survivin index) had a strong reverse association with survival time of patients. In particular, the survivin index correlated with patient survival in low grade gliomas.

Materials and methods

Cell culture

Human fibroblast, SK-N-SH (human neuroblastoma), HeLa (human uterin cervix epitheloid carcinoma), SNB-19 (human glioblastoma), FDCP-1 (mouse bonemarrow), and CHO K-1 (Chinese hamster ovary) were cultured in Dulbecco's modified Eagle medium/Ham's F12 (Life Technologies, Rockville, MD, USA) containing 10% fetal bovine serum with penicillin-streptomycin. Jurkat (human T cell leukemia) cells were cultured in RPMI1640 (Life Technologies) containing 10% fetal bovine serum with penicillin-streptomycin. Free from microbiological contamination was confirmed with PCR procedure (Takara, Tokyo, Japan).

Antiserum preparation

Survivin cDNA was obtained from SK-N-SH by the reverse transcription-PCR method with a pair of primers, 5′-NNGAATTCAATCCATGGCA GCCAGCTG and 5′-NNGAATTCAATGGGTG CCCCGACGTTG (N means any of the four nucleotides). On digestion with *Eco*RI, the resultant fragment was inserted into pProEx3 GST (Life Technologies) and sequenced to confirm accurate the full-length survivin cDNA. Overexpression and purification of a fusion protein of survivin with glutathione S-transferase (GST) in *Escherichia coli* were performed by a method described previously [21]. Rabbits were immunized with the purified protein with Freund's adjuvant of a mixture of 1:1 (Life Technologies).

Western blot analysis

Total cell lysates were separated on a 12.5% SDS-polyacrylamide gel electrophoresis and transferred onto poly-vinyl difluoride membrane (NEN, Boston, MA, USA). The membrane was blocked with 10% fetal bovine serum in Tris buffered saline (TBS) for 1 h, and then incubated with diluted anti-survivin antiserum in TBS with 0.2% Tween-20 (TBS-T) at 4 °C overnight. After a wash with TBS-T, the membrane was incubated with alkaline phosphatase-conjugated anti-rabbit IgG (Cappel, Aurora, OH, USA) and specific bands were visualized with AttoPhos substrate (Roche, Mannheim, Germany).

Immunocytochemistry

HeLa and human fibroblast cells were cultured on 4-well plastic dishes (SonicSeal slide, Nalge Nunc, Rochester, NY, USA). The cells were rinsed with phosphate buffered saline (PBS) and fixed in 4% paraformaldehyde in PBS. After a wash with PBS, the cells were incubated 30 min in 0.2% Triton X-100, 30 min in a blocking buffer (3% bovine serum albumin and 3% goat serum in PBS), and overnight at 4 °C in a blocking buffer containing anti-survivin antiserum (1:250). After another wash with PBS, the cells were incubated in a blocking buffer containing BODIPY FL goat anti-mouse IgG (1:500, Molecular Probes, Eugene, OR, USA) for 1 h and imaged with a confocal scanning microscope, the FLUOROVIEW FV/300 (Olympus, Tokyo, Japan).

Tissue processing and clinical data

There were 37 gliomas from 1994 to 2001 and 29 of these were suitable for this analysis. We prepared glioma samples from 29 patients [17 males and 12 females, age from 6 to 80 (mean 45.4) at the time of diagnosis; Table 1] who were operated with craniotomy, excepted biopsy, with informed consent. The samples were selectively collected from center zone of the tumor, quickly frozen, kept at −80 °C until used, fixed with formalin, and embedded in paraffin. Sections (4 μm) were used for immunohistochemistry and the classification of grades according to WHO guidelines diagnosed by two or more pathologists and neurosurgeons. Clinical data were obtained from the hospital records including age, sex, and survival time from the initial operation. Follow-up was available for all patients.

Immunohistochemistry

For immunostaining with anti-survivin antiserum, the 4-μm sections were stained using the Ventana NexES

Table 1. Characteristics in glioma patients[a]

No.	Age	Sex	WHO grade	MIB-1 index (%)	Survivin index (%)	Resection	Location	Depth	Survival days[b]	Out-come
1	30	male	2	5	85	subtotal	Temporal	sup[d]	2618	alive
2	40	female	2	5	75	total	Frontal	sup	2280	alive
3	10	male	2	n.d.[c]	65	total	Cerebellum	sup	2268	alive
4	26	female	2	5	65	total	Frontal	deep	2025	alive
5	27	female	2	25	80	subtotal	Pons	deep	246	dead
6	45	male	2	0	45	total	Frontal	deep	1550	alive
7	55	male	2	10	95	total	Frontal	deep	777	dead
8	29	male	2	n.d.	40	total	Pariental	sup	212	dead
9	50	male	2	5	80	subtotal	Frontal	deep	62	dead
10	46	male	3	5	65	subtotal	Frontal	deep	1505	alive
11	12	female	3	15	90	total	Frontal	deep	825	dead
12	6	female	3	35	90	subtotal	Pons	deep	150	dead
13	64	male	3	n.d.	85	subtotal	Frontal	sup	636	dead
14	64	male	3	0	85	subtotal	Frontal	deep	438	dead
15	21	male	3	5	35	total	Pons	deep	1173	dead
16	58	male	3	n.d.	95	subtotal	Frontal	deep	220	dead
17	23	male	3	15	85	total	Frontal	deep	425	alive
18	69	male	3	20	95	subtotal	Temporal	deep	336	dead
19	74	female	3	5	80	subtotal	Pariental	sup	102	alive
20	54	female	3	5	85	subtotal	Pariental	deep	180	dead
21	46	male	3	5	85	total	Frontal	deep	415	dead
22	54	male	4	n.d.	55	subtotal	Frontal	deep	374	dead
23	31	male	4	n.d.	80	subtotal	Frontal	deep	118	dead
24	78	male	4	n.d.	95	subtotal	Frontal	sup	47	dead
25	54	female	4	20	100	total	Occipital	sup	247	dead
26	80	female	4	55	90	subtotal	Frontal	deep	48	dead
27	79	female	4	55	90	subtotal	Frontal	deep	422	dead
28	11	female	4	n.d.	85	total	Cerebellum	sup	115	dead
29	80	female	4	55	85	subtotal	Frontal	sup	127	dead

[a]All samples were resected with craniotomy, excepted biopsy samples. [b]Survivial days are from the first operation. [c]Not determined. [d]Superficial.

Staining System (Ventana, Tucson, AZ, USA) and all products without the anti-survivin antiserum needed for subsequent steps were supplied by the manufacture (Ventana). Sections were deparaffinized and heated with CC1 solution (denature buffer; Ventana) for 1 h. After 32-min incubation at 37 °C with the anti-survivin antiserum (1:250), sections were further incubated for another 10 min at 37 °C with a secondary biotinylated antibody and then with avidin-peroxidase for another 10 min; 3′, 3-diaminobenzidine was used as the chromogen. Slides were counterstained in Mayer hematoxylin, dehydrated, and mounted. Immunostaining with MIB-1 (1:50 dilution, Immunotech, Westbrook, ME, USA) for detection of Ki-67 antigen was performed as described previously [4,22]. Stained sections were observed under the microscope. Survivin and MIB-1 indexes were determined as the percentage of immunostained cells per 200 cells × 5 fields per section.

Statistical analysis

Statistical analyses were performed using Stat View for Macintosh Version 5.0 (SAS Institute Inc., Cary, NC, USA). The survivin index, the MIB-1 index, and survival times were subjected to linear regression analysis. Survival was plotted, and survival time was estimated by the Kaplan-Meier method. The survival times and the strength of associations between categories were compared with the log-rank test (Mantel-Cox) for univariate analysis. For multivariate analysis, tumor location (temporal, frontal, pariental, occipital, pons or cerebellum), depth (deep or superficial), age (young ≤ 20 year-old, $20 <$ middle < 65, or $65 \leq$ old), survivin index (higher 17 samples, or lower 12 samples), and MIB-1 index (higher 10 samples or lower 11 samples) were compared with survival times. A $P < 0.05$ was considered significant.

Results

Antisera specific to the survivin protein

To examine the expression of survivin in patients immunohistochemically, rabbit antisera were raised against GST-survivin fusion protein. The diluted sera (1:10000) specifically stained only major 16.5-kDa and minor 14-kDa bands in Western blots of 3 μg total cell lysate from cultured GBM, SNB-19 (Figure 1a, Lane 1–2). A 16.5-kDa specific band of survivin was also detected in Western blots of 1 μg lysate from other cultured cells (Figure 1a, Lane 3–5). Immunocytochemical staining of HeLa cells with the obtained antiserum revealed that survivin immunoreactivity was associated with the centrosome, mitotic spindle and midbody (Figure 1b), as previously described [13,16,17].

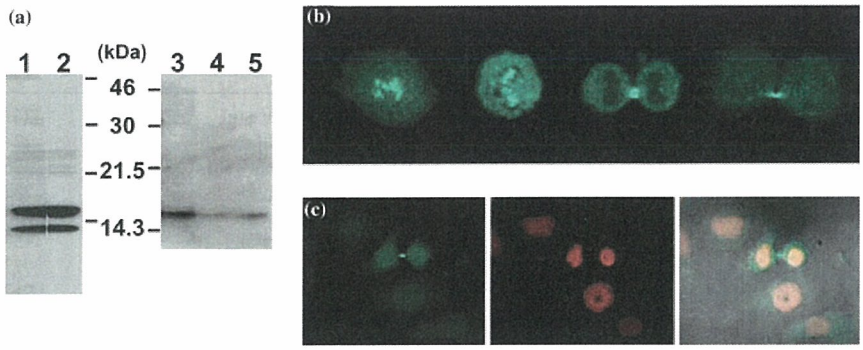

Figure 1. Characterization of anti-survivin antiserum. (a) Western blotting analysis for survivin in each cell lysate from SNB-19 (glioma, Lane 1 and 2), FDCP-1 (mouse bone marrow, Lane 3), Jurkat (Lane 4), and CHO K-1 (Chinese hamster ovary, Lane 5). Three μg per lane (Lane 1 and 2) or 1 μg per lane (Lane 3–5) of lysate was subjected and stained with 1:5000 diluted sera (Lane 1, 3–5) or with 1:10000 diluted sera (Lane 2). (b) HeLa cells in mitosis were immunohistochemically stained with 1:1000 diluted sera. Original magnification, × 600. (c) Human primary fibroblasts were immunohistochemically stained with 1:1000 diluted sera. Left panel; stained with anti-survivin serum, middle; with propidium iodine, and right panel; merge. Original magnification, ×600.

Furthermore, survivin localized in the midbody of primary cultured fibroblast was also detected as shown in Figure 1c, suggesting that the antiserum preparation immunodetects survivin in not only malignant tumors but also normal replicating cells, and is strong enough in immuno-reactivity and purity for further experiments.

Distribution patterns of survivin in glioma

Automated immunohistochemistry was performed on paraffin-embedded sections prepared from surgical specimens with anti-survivin antiserum (1:250) using the Ventana IHC staining system. Stained sections from glioma patients in various histological grades are shown in Figure 2A, C, and E. No positive immunoreactivity was detected without antiserum, and survivin expression was undetectable around gliosis (Figure 2G) and in normal tissues (Figure 2H). All specimens (n = 29) from glioma patients contained positive cells, but the percentage of positive cells (designated as the survivin index) was heterogeneous among grades, which were determined with histopathological diagnosis (Figure 3a). The mean percentage of immunoreactive cells in each specimen was 70.0% in low grade astrocytoma (grade II, 9 specimens), 81.3% in anaplastic astrocytoma (grade III, 12 specimens), and 85.0% in GBM (grade IV, 8 specimens). Thus, the immunoreactivity of survivin is a highly sensitive marker for glioma.

Progonostic value of survivin index for glioma

To evaluate the prognostic value of the survivin index, the correlation of survival time of patients with the survivin index for all grades of glioma was investigated using a scatter plot diagram (Figure 4a). An increasing percentage of survivin-positive cells was reversely associated with the survival time ($P = 0.049$). The patients were further divided in two groups, high (index ≥ 80) and low (80 > index), and then the survival curve of the groups was calculated by the Kaplan-Meier method (Figure 5a). Survival times were significantly shortened ($P = 0.003$) for patients whose survivin index was high (mean survival time = 349 days) compared with those whose index was low (mean survival time = 953 days).

Lower correlation between survivin and MIB-1 indexes in low-grade gliomas

Ki-67 antigen, which is detected by MIB-1 antibody, is a nuclear protein complex and the percentage of MIB-1- positive cells (MIB-1 index) is widely used for the diagnosis of many malignant tumors including glioma [5,8,23]. Then, we investigated the correlation between survivin and MIB-1 indexes in consecutive sections (Figure 2). A linear positive correlation between them was not significant, but weak correlation was noted essentially (Figure 6, $P = 0.065$), whereas an increasing percentage of MIB-1-positive cells was still associated with worse survival (Figure 4b, $P = 0.037$). However, as shown in Figure 3b, MIB-1 indexes in anaplastic astrocytoma were shown to be as low as those in low grade astrocytoma, whereas survivin indexes in anaplastic astrocytoma were similar to those in GBM, indicating that the survivin index would be a more sensitive marker for low-grade gliomas than the MIB-1 index. Then, patients were divided into two groups based on the MIB-1 index, high (index ≥ 10) and low (10 > index), and then the survival curve of each group was obtained by the Kaplan-Meier method. In total, survival times were significantly shortened (Figure 5b, $P = 0.033$) for patients whose MIB-1 index was high (mean survival time = 398 days) compared with those whose index was low (mean survival time = 821 days). However, in low-grade gliomas, the difference in survival times between the high and low MIB-1 indexes was not significant (Figure 5d, $P = 0.092$). At that time, in low-grade gliomas, the difference in survival times between the high and low survivin indexes was still significant (Figure 5c, $P = 0.007$).

Finally, we compared the difference in survival times among age of patients, tumor location, depth, the survivin index, and the MIB-1 index by a multivariate analysis. The suvivin index was significantly associated

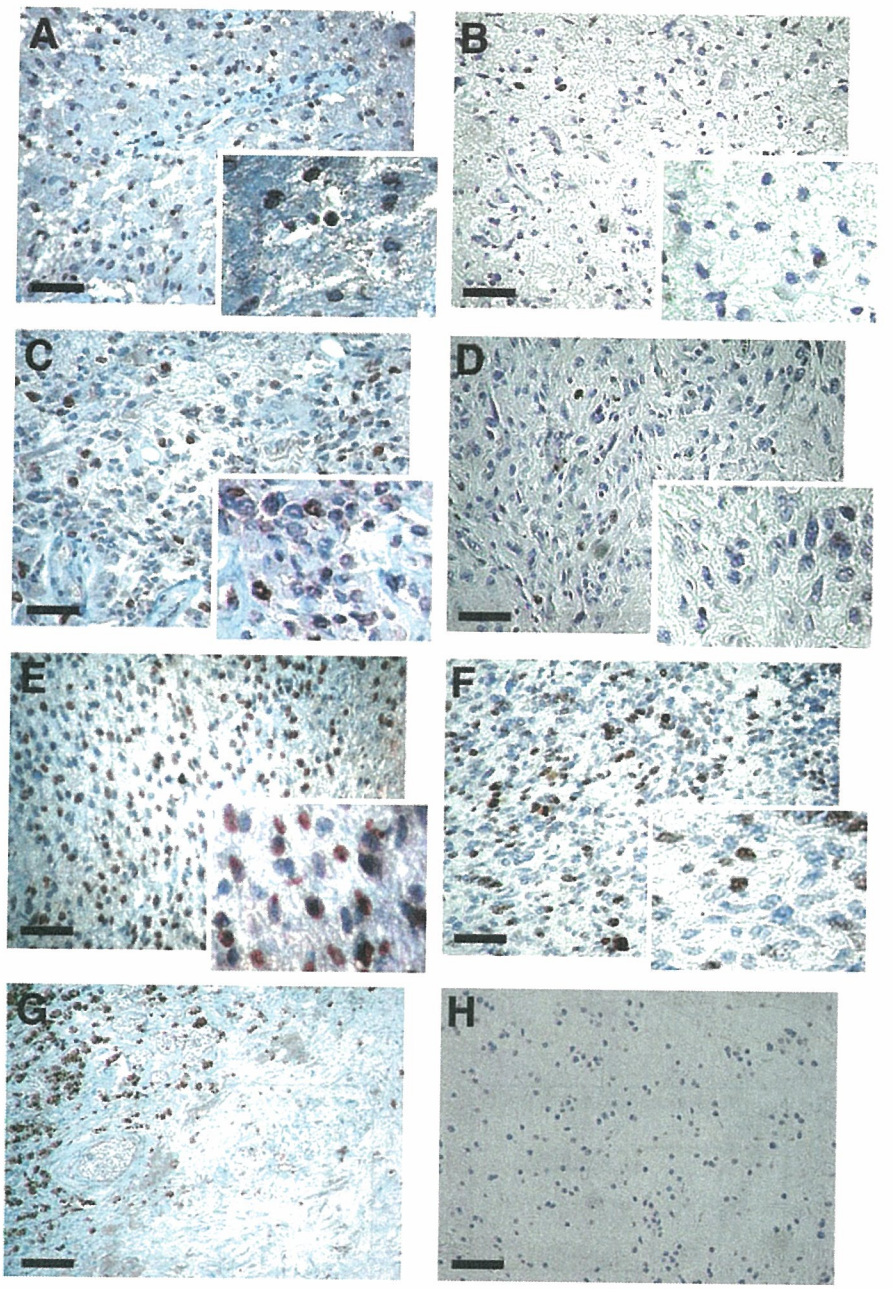

Figure 2. Immunostaining of gliomas. Immunohistochemical staining for surgical sections staining with 1:250 diluted anti-survivin serum (A, C, E, G and H), using the Ventana NexES Staining System (Ventana, Tucson, AZ). Immunohistochemical staining for surgical sections with 1:50 diluted anti-Ki-67 serum (B, D and F). A and B; low grade astrocytoma. C and D; anaplastic astrocytoma. E, F and G; GBM. G; local invasion of GBM and around gliosis. H; normal brain tissue. Original magnification, ×200 and ×400 (insets). Bars are 100 μm.

with the survival times ($P = 0.036$), while other characteristics were not (location: $P = 0.922$, depth: $P = 0.402$, age: $P = 0.866$ and MIB-1 index: $P = 0.404$). Taken together, these findings strongly suggest that the survivin index is a useful tool for the prognosis of histologically low-grade gliomas.

Discussion

In this study, we demonstrated that gliomas highly expressed survivin and that the percentage of immunoreactive cells (survivin index) had a strong inverse association with the survival of patients. In particular, the survivin index correlated with the survival of low grade gliomas, suggesting that the index would be useful for a clinical prognosis.

Our antiserum raised against the GST-survivin fusion protein was highly specific and sensitive to the survivin protein (Figure 1). Western blotting of cell lysates revealed that both the 16.5-kDa full- length and 14-kDa alternatively spliced products were expressed in cultured GBM SNB-19 (Figure 1a, Lane 1–2). We used a survivin-specific RT-PCR and identified that a 14-kDa band

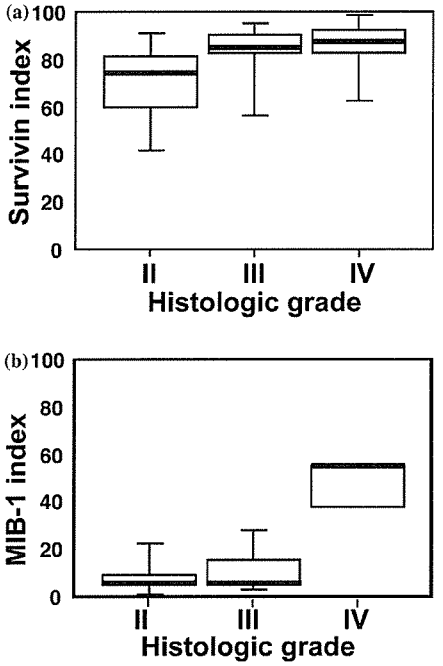

Figure 3. Correlation of histological grade with indexes. Correlations of survivin (a) and MIB-1 (b) indexes vs. histological grade are demonstrated. The difference between grade II and grade III is more obvious in the survivin index than MIB-1 index. Data are presented as the median (solid line), 25th and 75th percentiles (vertical boxes) and 10th and 90th percentiles (error bars).

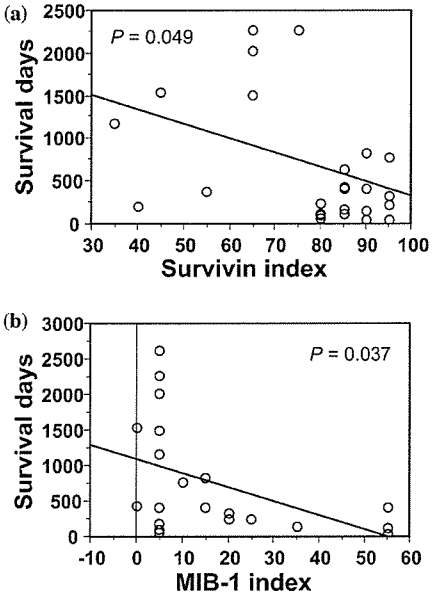

Figure 4. Correlation of survivin and MIB-1 indexes with survival times of patients. Survival time is the period until patients died from the first operation, the index is the percentage of immunoreactive cells in tumor cells in each surgical specimen. Survivin (a) and MIB-1 indexes (b) vs. survival time in each patient (each dot) are demonstrated.

was survivin-ΔEx3 and 10–40 % of survivin mRNA was survivin-ΔEx3 (unpublished results). However, functions of the regulatory balance between them are unknown [21,24]. Immunocytochemistry with anti-survivin antiserum clearly demonstrated that both the immortal cell line and primary cultured fibroblasts expressed survivin in a cell-cycle dependent fashion (Figure 1b and c). However, immunological signals in highly proliferative cells, such as HeLa cells, were stronger than those in

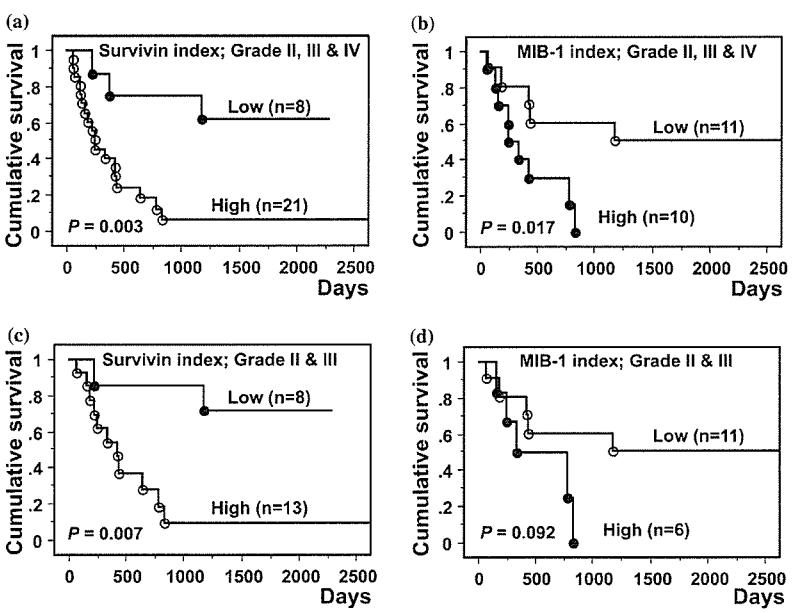

Figure 5. Kaplan-Meier plots in survivin and MIB-1 indexes. (a and c) Comulative survival rate for survivin index. Patients were separated into two groups, high (index ≥ 80) and low (80 > index). a; patients with all grade gliomas. c; all patients except those with GBM (grade IV). (b and d) Comulative survival rate for the MIB-1 index. Patients were separated into two groups, high (index ≥ 10) and low (10 > index). b; patients with all grade glioma. d; all patients except those with GBM (grade IV). Note that the survivin index is significant for survival times in glioma patients except those with GBM, but the MIB-1 index is not.

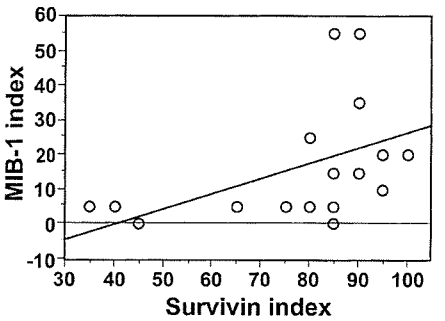

Figure 6. Correlation between the survivin index and MIB-1 index.

primary cells. Then, the anti-survivin antiserum was confirmed for sensitivity and purity in immunohistochemical studies.

Large numbers of cells in gliomas of all grades were survivin- positive by the immunohistochemical staining (Figure 2). Positive cells having weak survivin immunoreactivity in cytosol, but not in the nucleus, were observed. Recent findings of Fortugno et al. have indicated that endogenous survivin exists in strikingly different subcellular pools, comprising a predominant cytosolic fraction and a smaller nuclear pool [13]. Therefore, an immunohistochemically detectable amount of survivin was accumulated not only in the nucleus, but also in cytosol of gliomas. In addition, the immunoreactivity of survivin is a highly sensitive marker for glioma, providing the narrow window of the survivin index compared with the MIB-1. We found that the proportion of gliomas with a high survivin index was greatest in GBM (85.0% (SD 13.6%)) and lowest in low-grade astrocytomas (70.0% (18.2%)). The survivin index in anaplastic astrocytoma (81.3% (16.5%)) was not significantly different from that in GBM. On the other hand, the MIB-1 index in anaplastic astrocytoma (11.0%) was not significantly different from that in low-grade astrocytomas (7.9%), indicating that the survivin index is a more sensitive marker than the MIB-1 index for all grades of gliomas.

It was reported that the survivin expression in neuroblastoma cell lines was strongly down-regulated during the induction of apoptosis and the expression of exogenous survivin prevented cell death. Survivin is thought to inhibit apoptosis by directly inhibiting terminal effectors caspase-3 and -7, and to maintain the normal function of the mitotic apparatus [12,15]. Thus, in glioma, survivin may enhance cell survival and proliferation, and then, its expression is associated reversely with prognostic factors.

Significant numbers of patients with anaplastic astrocytoma and low grade astrocytoma rapidly developed more malignant tumors. Since standard histological techniques do not precisely predict which tumors will undergo rapid malignant progression, it is difficult to give accurate prognostic information to patients. As shown in Figure 4a, the survivin index was associated with a significant decrease in the survival of patients nevertheless the high SD values. When gliomas were analyzed separately from GBM, the increased survivin index remained an important prognostic variable (Figure 5c). These results suggest that the survivin index is more significant than the histological grading to the prognosis for gliomas. Furthermore, the MIB-1 index has been reported to be clinically useful in the prognosis. However, the MIB-1 index did not predict prognostic reliability in gliomas separated from GBM (Figure 5d). Indeed, in several studies, the MIB-1 index did not correlate with survival in the low grade gliomas [9,10,23]. Finally, the survival index was confirmed to be significantly associated with the survival times by the multivariate analysis. Thus, this study proposed a possibility that the survivin index, which is correlated with the survival of low grade gliomas, will be a powerful tool for a clinical prognosis. It will be required to analyze more samples to reveal its usefulness.

References

1. Tanwar MK, Gilbert MR, Holland EC: Gene expression microarray analysis reveals YKL-40 to be a potential serum marker for malignant character in human glioma. Cancer Res 62: 4364–4368, 2002
2. Grzybicki DM, Moore SA: Implications of prognostic markers in brain tumors. Clin Lab Med 19: 833–847, 1999
3. Heesters MA, Koudstaal J, Go KG, Molenaar WM: Analysis of proliferation and apoptosis in brain gliomas; prognostic and clinical value. J Neuro-oncol 44: 255–266, 1999
4. Ralte AM, Sharma MC, Karak AK, Mehta VS, Sarkar C: Clinicopathological features, MIB-1 labeling index and apoptotic index in recurrent astrocytic tumors. Pathol Oncol Res 7: 267–278, 2001
5. Schiffer D, Cavalla P, Chio A, Richiardi P, Giordana MT: Proliferative activity and prognosis of low-grade astrocytomas. J Neuro-oncol 34: 31–35, 1997
6. Shiraishi S, Tada K, Nakamura H, Kochi M, Saya H, Kuratsu J, Ushio Y: Influence of p53 mutations on prognosis of patients with glioblastoma. Cancer 95: 249–257, 2002
7. Ishii N, Tada M, Hamou MF: Cells with TP53 mutations in low grade astrocytic tumors evolve clonally to malignancy and are an unfavorable factor. Oncogene 18: 5870–5878, 1999
8. Di X, Nishizaki T, Harada K, Kajiwara K, Nakayama H, Ito H: Proliferative potentials of glioma cells and vascular components determined with monoclonal antibody MIB-1. J Exp Clin Cancer Res 16: 153–157, 1997
9. Vaquero J, Zurita M, Coca S, Oya S: Imbalance between apostain expression and proliferative index can predict survival in primary glioblastoma. Acta Neurochir (Wien), 144: 151–155, 2002
10. Fisher BJ, Naumova E, Leighton CC, Naumov GN, Kerklviet N, Fortin D, Macdonald DR, Cairncross JG, Bauman GS, Stitt L: Ki-67: a prognostic factor for low-grade glioma? Int J Radiat Oncol Biol Phys 52: 996–1001, 2002
11. Takahashi H, Herlyn D, Atkinson B, Powe J, Rodeck U, Alavi A, Bruce DA, Koprowski H: Radioimmunodetection of human glioma xenografts by monoclonal antibody to epidermal growth factor receptor. Cancer Res 47: 3847–3850, 1987
12. Shankar SL, Mani S, O'Guin KN, Kandimalla ER, Agrawal S, Shafit-Zagardo B: Survivin inhibition induces human neural tumor cell death through caspase-independent and-dependent pathways. J Neurochem 79: 426–436, 2001
13. Fortugno P, Wall NR, Giodini A, O'Connor DS, Plescia J, Padgett KM, Tognin S, Marchisio PC, Altieri DC: Survivin exists in immunochemically distinct subcellular pools and is involved in spindle microtubule function. J Cell Sci 115: 575–585, 2002
14. Yamamoto T, Tanigawa N: The role of survivin as a new target of diagnosis and treatment in human cancer. Med Electron Microsc 34: 207–212, 2001

15. Islam A, Kageyama H, Takada N, Kawamoto T, Takayasu H, Isogai E, Ohira M, Hashizume K, Kobayashi H, Kaneko Y, Nakagawara A: High expression of Survivin, mapped to 17q25, is significantly associated with poor prognostic factors and promotes cell survival in human neuroblastoma. Oncogene 19: 617–623, 2000
16. Li F, Ambrosini G, Chu EY, Plescia J, Tognin S, Marchisio PC, Altieri DC: Control of apoptosis and mitotic spindle checkpoint by surviving. Nature 396: 580–584, 1998
17. Ambrosini G, Adida C, Sirugo G, Altieri DC: Induction of apoptosis and inhibition of cell proliferation by survivin gene targeting. J Biol Chem 273: 11177–11182, 1998
18. Chiodino C, Cesinaro AM, Ottani D, Fantini F, Giannetti A, Trentini GP, Pincelli C: Expression of the novel inhibitor of apoptosis survivin in normal and neoplastic skin. J Invest Dermatol 113: 415–418, 1999
19. Konno R, Yamakawa H, Utsunomiya H, Ito K, Sato S, Yajima A: Expression of survivin and Bcl-2 in the normal human endometrium. Mol Hum Reprod 6: 529–534, 2000
20. Chakravarti A, Noll E, Black PM, Finkelstein DF, Finkelstein DM, Dyson NJ, Loeffler JS: Quantitatively determined survivin expression levels are of prognostic value in human gliomas. J Clin Oncol 20: 1063–1068, 2002
21. Mahotka C, Wenzel M, Soringer E, Gabbert HE, Gerharz CD: Survivin-ΔEx3 and survivin-2B: Two novel splice variants of the apoptosis inhibitor survivin with different antiapoptotic properties. Cancer Res 59: 6097–6102, 1999
22. Enestrom S, Vavruch L, Franlund B, Nordenskjold B: Ki-67 antigen expression as a prognostic factor in primary and recurrent astrocytomas. Neurochorirurgie 44: 25–30, 1998
23. Marie D, Liu Y, Moore SA, Brown HG, Silverman JF, D'Amico F, Raab SS: Interobserver variability associated with the MIB-1 labeling index: high levels suggest limited prognostic usefulness for patients with primary brain tumors. Cancer 92: 2720–2726, 2001
24. Conway EM, Pollefeyt S, Cornelissen J, DeBaere I, Steiner-Mosonyi M, Ong K, Baens M, Collen D, Schuh AC: Three differentially expressed survivin cDNA variants encode proteins with distinct antiapoptotic functions. Blood 95: 1435–1442, 2000

Address for offprints: Shigeo Ohta, Department of Biochemistry and Cell Biology, Institute of Development and Aging Sciences, Graduate School of Medicine, Nippon Medical School, 1-396 Kosugi-cho, Nakahara-ku, Kawasaki, Kanagawa, Japan 211-8533; Tel.: +81-44-733-9167; Fax: +81-44-733-9168; E-mail: ohta@nms.ac.jp

JCS ePress online publication date 1 November 2005

MIDAS/GPP34, a nuclear gene product, regulates total mitochondrial mass in response to mitochondrial dysfunction

Naomi Nakashima-Kamimura[1], Sadamitsu Asoh[1], Yoshitomo Ishibashi[1], Yuri Mukai[1,*], Yujiro Shidara[1,2], Hideaki Oda[2], Kae Munakata[3], Yu-ichi Goto[3] and Shigeo Ohta[1,‡]

[1]Department of Biochemistry and Cell Biology, Institute of Development and Aging Sciences, Graduate School of Medicine, Nippon Medical School, 1-396 Kosugi-cho, Kawasaki, Kanagawa, 211-8533, Japan
[2]Department of Pathology, Tokyo Women's Medical University, School of Medicine, Shinjuku-ku, Tokyo, 162-8666, Japan
[3]Department of Mental Retardation and Birth Defect Research, National Institute of Neuroscience, NCNP, Kodaira, Tokyo, 187-8502, Japan
*Present address: Computational Biology Research Center (CBRC), National Institute of Advanced Industrial Science and Technology (AIST), Koutou-ku, Tokyo, 135-0064, Japan
‡Author for correspondence (e-mail:ohta@nms.ac.jp)

Accepted 15 August 2005
Journal of Cell Science 118, 000-000 Published by The Company of Biologists 2005
doi:10.1242/jcs.02645

Summary

To investigate the regulatory system in mitochondrial biogenesis involving crosstalk between the mitochondria and nucleus, we found a factor named MIDAS (mitochondrial DNA absence sensitive factor) whose expression was enhanced by the absence of mitochondrial DNA (mtDNA). In patients with mitochondrial diseases, MIDAS expression was increased only in dysfunctional muscle fibers. A majority of MIDAS localized to mitochondria with a small fraction in the Golgi apparatus in HeLa cells. To investigate the function of MIDAS, we stably transfected HeLa cells with an expression vector carrying *MIDAS* cDNA or siRNA. Cells expressing the MIDAS protein and the siRNA constitutively showed an increase and decrease in the total mass of mitochondria, respectively, accompanying the regulation of a mitochondria-specific phospholipid, cardiolipin. In contrast, amounts of the mitochondrial DNA, RNA and proteins did not depend upon MIDAS. Thus, MIDAS is involved in the regulation of mitochondrial lipids, leading to increases of total mitochondrial mass in response to mitochondrial dysfunction.

Supplementary material available online at
http://jcs.biologists.org/cgi/content/full/118/22/5357/DC1

Key words: Mitochondria, Mitochondrial mass, Cardiolipin, Mitochondrial DNA, Mitochondrial disease, Golgi apparatus

Introduction

The mitochondrion is the center of energy metabolism in eukaryotes and has recently been recognized as a multifunctional organelle (Ohta, 2003). It is involved in the regulation of apoptosis as a reservoir of signals, regulators and executioners (Kroemer and Reed, 2000; Green and Kroemer, 2004). In addition, it functions as a source of reactive oxygen species, which are believed to cause many lifestyle-related diseases, neurodegenerative diseases, cancer and aging (Kowaltowski and Vercesi, 1999; Cortopassi and Wong, 1999; Melov, 2000). Thus, mitochondria are essential in many aspects of medicine as well as cell biology.

Depending on cell type, energy demands and physiological conditions, mitochondria vary in number, mass and morphology (Attardi and Schatz, 1988; Yaffe, 1999; Collins et al., 2002; Nisoli et al., 2003). The proliferation of cells usually accompanies an increase in mitochondria. However, an increase in number of mitochondria is not distinctly coordinated with the cell cycle. For example, muscle mitochondria increase in response to exercise, independently of cell division (Brunk, 1981; Moyes et al., 1997). Exposure to a low-temperature environment or cultivation in glucose-deprived medium induces a marked increase in mitochondrial mass (Klaus et al., 1991; Weber et al., 2002). In addition, mitochondria increase in response to external stimuli with a wide range of substances including benzodiazepine, phorbol esters, calcium fluxes (Bereiter-Hahn and Voth, 1994; Vorobjev and Zorov, 1983; Muller-Hocker et al., 1986; Kawahara et al., 1991), thyroid hormones (Goglia et al., 1999) and nitric oxide (NO) (Nisoli et al., 2004). Mitochondrial numbers also increase in response to internal stimuli, such as the mitochondrial dysfunction caused by pathogenic mtDNA mutations (Schon, 2000; Wallace, 1999; Moraes et al., 1992). An increase in mitochondrial mass was observed in mitochondrial transcription factor A (*Tfam*) knockout mice, which have depleted mtDNA (Hansson et al., 2004).

As nuclear genes encode most mitochondrial proteins, including the enzymes and cofactors required for the transcription and replication of mtDNA, mitochondrial biogenesis depends on a distinct crosstalk between two physically separated genetic systems (Garesse and Vallejo, 2001). Recently, the pathway that links external physiological stimuli to the regulation of mitochondrial biogenesis and function has been studied. Several transcription/replication factors directly regulate mitochondrial genes and the

Journal of Cell Science

coordination of these factors into a programmed response to the environment was reported (Scarpulla, 2002).

However, the nature of mitochondrial biogenesis in response to internal stimuli is poorly understood. Mitochondrial stress results in enhanced expression of sarcoplasmic reticular ryanodine receptor-1 and some Ca^{2+}-responsive transcription factors (Biswas et al., 1999). Several tumor-specific markers are overexpressed in cells subjected to mitochondrial genetic as well as metabolic stress (Amuthan et al., 2001). Moreover, we have reported that expression of the apoptosis-mediator Fas is enhanced by dysfunctional mitochondria (Asoh et al., 1996). However, no one has reported on the mammalian factors, in response to a signal from mitochondria to the nucleus, which are involved in the stimulation of mitochondrial growth. Notably, the molecular mechanism regulating the biogenesis of mitochondrial lipids is poorly understood.

In this study, we identified factors whose expression was enhanced by depletion of mtDNA. One of them was found to increase total mitochondrial mass without a pathogenic swelling, when overexpressed. Thus, the factor is involved in the accumulation of mitochondria in response to mitochondrial dysfunction.

Materials and Methods

Cells and culture

EB8 and Ft2-11 were described previously (Hayashi et al., 1991; Hayashi et al., 1994). EB8 is a clone, derived from HeLa cells, completely lacking mtDNA, whereas Ft2-11 was constructed by transferring wild-type mtDNA into EB8 so that Ft-2-11 has the same nucleus as EB8. Stable transfectants expressing MIDAS constitutively were constructed from HeLa cells by transfection with *MIDAS* cDNA under the control of the CMV promoter or its empty vector (pCMV-SPORT; Life Technologies).

Stable transfectants expressing siRNA of *MIDAS* were constructed from HeLa cells by transfection with the pSilencer vector (Ambion) with inserts targeting *MIDAS* (5′-AAGCTTTTCCAAAAAAGTGG-AATGTCTGAAGGCCATCTCTTGAATGGCCTTCAGACATTCC-ACGGGATCC-3′) or a random sequence.

HeLa cells and stable transfectants were cultured in DMEM/F-12 (1:1) (Gibco-BRL) supplemented with 10% FBS and 1% penicillin/streptomycin (Gibco-BRL).

Construction of Myc-tagged MIDAS

To insert the Myc tag at the N-terminus of MIDAS, an *Eco*RI site was generated at the 5′ end of the *MIDAS* coding sequence by PCR and was cloned into the pCMV-SPORT vector. An oligonucleotide encoding MEQKLISEEDLNS (Myc tag sequence underlined) was inserted at the newly generated *Eco*RI site of *MIDAS*. To construct the Myc tag at the C-terminus of MIDAS, a *Bam*HI site was generated at the 3′ end of the coding sequence and an oligonucleotide encoding DPEQKLISEEDL was inserted.

Differential display

Poly(A)$^+$ RNA was purified from Ft2-11 and EB8 and reverse transcribed. Resultant cDNAs were amplified using arbitrary primer sets, followed by 5% PAGE. The gel was stained with Vistra Green (Amersham Biosciences) and visualized with a Fluoro Imager (Molecular Dynamics) (Liang and Pardee, 1992).

Antibodies

Anti-MIDAS polyclonal rabbit antiserum was raised against His-tagged MIDAS expressed in *Escherichia coli*. Anti-MIDAS antibody was affinity purified by binding to the MIDAS protein isolated by SDS-PAGE, followed by transfer onto a PVDF membrane. Anti-Tom20 and anti-Tom40 were gifts from K. Mihara, Kyushu University, Japan. Other antibodies were purchased as follows: anti-actin (clone AC-40) and anti-β-tubulin from Sigma; anti-p230 antibody and anti-Syntaxin6 from BD Biosciences; anti-Hsc70 antibody from Santa Cruz; anti-Hsp60 from MBL; anti-cytochrome c antibody and anti-Cox4 from Clontech; and anti-SDH70, anti-SDH30, anti-COX I and anti-COX II antibodies from Molecular Probes.

Immunohistochemical staining of muscle sections

Biopsy samples were obtained from the biceps brachii muscle with informed consent and then frozen in isopentane and liquid nitrogen. Frozen sections 6 μm thick were stained histochemically and immunologically. Activities of SDH and COX were visualized as described previously (Hasegawa et al., 1991; Dubowitz, 1985). The expression of MIDAS was detected with anti-MIDAS antibody. The polyclonal antibody against MIDAS was diluted 500-fold with 10% BSA in PBS and incubated with sections for 5 hours at 37°C and then MIDAS was detected with DAB using an indirect streptavidin-biotin immunohistochemical method, according to the manufacturer's protocol (Histofine, Nichirei, Co. Ltd., Tokyo, Japan). The MIDAS protein expressed was semi-quantified by the density of staining.

Immunocytostaining of cultured cells

Cultured cells were fixed with 4% paraformaldehyde in PBS for 20 minutes at room temperature. After a wash with PBS, they were treated with 5% acetic acid in ethanol for 10 minutes at –20°C to permeabilize membranes, then incubated in a blocking buffer (3% BSA and 3% goat serum in PBS) and overnight at 4°C in the blocking buffer containing primary antibody. After another wash with PBS, the cells were incubated in the blocking buffer containing labeled secondary antibody and visualized with a confocal laser-scanning microscope (Fluoview FV300, Olympus, Tokyo, Japan). As an alternative, we used another method described (Bell et al., 2001). In brief, cells were fixed for 10 minutes with 4% paraformaldehyde and 4% sucrose without treatment for permeabilization and incubated with primary antibody, followed by secondary antibody.

Subfractionation of HeLa cells

Cells were homogenized as described (Trounce et al., 1996). The homogenate was applied to a 7-35% (w/v) Nycodenz preformed continuous density gradient and centrifuged in a swinging-bucket rotor at 77,000 g_{AV} for 4 hours. The fractions were collected from the top of the gradient. The MIDAS protein was semi-quantified by the density of total bands in western blots. The sub-organellar fractionation of mitochondria (fraction number 15) was performed as described (Kanamori et al., 2003).

Electron microscopy

Cells were cultured on plastic dishes and fixed with 2% glutaraldehyde in PBS. Ultra-thin sections were stained with uranyl acetate and lead nitrate and examined with an H-7000 electron microscope (Hitachi, Tokyo, Japan).

Flow cytometry

Living transfectants were stained with 20 nM MitoTracker Red CMXRos (Molecular Probes) or 100 nM MitoTracker Green (Molecular Probes) for 30 minutes at 37°C, treated with trypsin and subjected to a flow cytometric analysis with an Epics Elite ESP (Coulter).

Three-dimensional imaging

Living cells were stained with 20 nM MitoTracker Red and 500 nM SYTO 16 (Molecular Probes) for 30 minutes at 37°C. The cells were scanned using 0.4 μm sections with the confocal laser-scanning microscope. Three-dimensional (3D) views were reconstructed with Fluoview software (Olympus) and volumes of the nucleus and mitochondria were calculated by summing fluorescent areas from each section using the NIH Image program (developed at the US National Institutes of Health and available on http://rsb.info.nih.gov./nih-image).

Separation of phospholipids

Total lipids were extracted from transfectants using methanol/chloroform as described (Folch et al., 1957). For the separation and detection of phospholipids, total lipids were injected into a HPLC system (model 616; Waters) fitted with a Wakosil 5Sil column (Wako, Tokyo, Japan). The mobile phase was a mixture of n-hexan, isopropanol, ethanol, acetic acid and 25 mM potassium phosphate buffer (pH 7.0) (146:282.5:50:0.3:31; v/v/v/v/v). The flow rate was 1 ml/minute. The elution of phospholipids was monitored at 205 nm with the UV detector (SPD-10A; Shimadzu). Retention times and quantities of phospholipids were determined using a phospholipid kit (Doosan Serdary Research Laboratory) as a standard.

Results

Cloning of genes that respond to a depletion of mtDNA

To identify nuclear genes that respond to a depletion of mtDNA, we screened for mRNA whose expression increased in cells lacking mtDNA using the differential mRNA display technique (Liang and Pardee, 1992) (Fig. 1A) by comparing mRNA populations in a HeLa derivative lacking mtDNA (EB8) (Hayashi et al., 1991) and control cybrid cells (Ft2-11) (Hayashi et al., 1994). Bands 1 and 2, which were stronger in EB8 than in Ft2-11 (Fig. 1A), were found to correspond to the apurinic/apyrimidinic endonuclease I (APE1/HAP1) (Demple et al., 1991) and DNA ligase III genes (Wei et al., 1995), respectively. The products of these genes are localized in mitochondria and involved in mtDNA repair (Kang and Hamasaki, 2002).

DNA sequencing distinguished the gene corresponding to the third band in Fig. 1A from the genes which have been so far identified to be involved in mitochondrial biogenesis, gene expression and metabolism. The full-length cDNA was isolated from a human brain cDNA library (Gibco-BRL) to confirm the increase in its mRNA (Fig. 1B,C) and its product (Fig. 1D,E) by northern and western blotting, respectively. We named this gene *MIDAS* (mitochondrial DNA absence sensitive factor), because the gene product was expressed in response to mtDNA depletion. Interestingly, the nucleotide sequence was identical to *GPP34* (GenBank accession no. AJ296152) whose product has been identified as a Golgi protein of unknown function(s) (Bell et al., 2001). In addition, MIDAS/GPP34 contains an isoform named GPP34R (GenBank accession no. AJ296153), which is highly homologous with MIDAS/GPP34 (supplementary material Fig. S1). In fact, GPP34R was expressed in cells with the HeLa nucleus as detected by northern blotting (supplementary material Fig. S2A). Interestingly, GPP34R was also expressed more abundantly in EB8 than in Ft2-11 (supplementary material Fig. S2A). The relative amount of GPP34R mRNA was semi-quantified by the TaqMan probe method and found to be less than 2% of that in

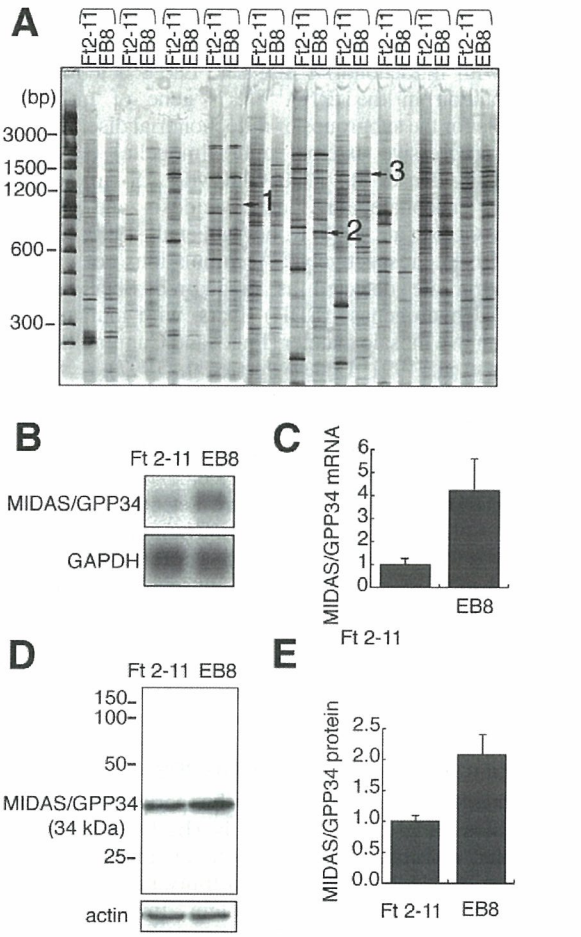

Fig. 1. Enhanced expression of MIDAS/GPP34 in EB8 (mtDNA-free HeLa cells). (A) Comparison of mRNA obtained from Ft2-11 with that from EB8 by differential display. EB8 lacks mtDNA whereas Ft2-11 is derived from EB8 but has wild-type mitochondria. Ten sets of arbitrarily primed PCR products were subjected to 5% PAGE. Three bands indicated by arrows were cloned and sequenced. Bands 1, 2 and 3 corresponded to apurinic/apyrimidinic endonuclease I, DNA ligase III and MIDAS/GPP34, respectively. (B) Northern blots of total RNA extracted from Ft2-11 and EB8 were hybridized with *GPP34*- and *GAPDH* (glyceraldehyde-3-phosphate dehydrogenase)-specific probes. (C) *GPP34* mRNA levels normalized to *GAPDH* levels based on the mean values±s.d. for three sets of northern blotting experiments (vertical bars). (D) Western blotting of Ft2-11 and EB8. Whole-cell lysates were separated by 12% SDS-PAGE and transferred onto a PVDF membrane. MIDAS/GPP34 was immunostained with anti-MIDAS antibody. (E) The MIDAS/GPP34 protein normalized against actin. Mean values of three sets of experiments are shown with s.d. (vertical bars).

MIDAS/GPP34 (supplementary material Fig. S2B). Therefore, we focused on the function of MIDAS/GPP34.

Specific expression of MIDAS/GPP34 in muscle fibers with abnormal mitochondria

Mitochondria accumulate in response to their own dysfunction

in mitochondrial diseases (Schon, 2000; Wallace, 1999). We examined the expression of MIDAS/GPP34 in muscle fibers of patients with mitochondrial diseases. Large deletions and a point mutation in the $tRNA^{Leu(UUR)}$ gene of mtDNA are responsible for the subgroups of mitochondrial diseases, CPEO (chronic progressive external ophthalmopelia) (Holt et al., 1988; Shoubridge et al., 1990) and MELAS (mitochondrial myopathy, encephalopathy, lactic acidosis and stroke-like episodes) (Goto et al., 1990; Kobayashi et al., 1990; Kobayashi et al., 1991), respectively. Accumulations of abnormal mitochondria are detected as ragged-red fibers and high succinate dehydrogenase (SDH) fibers, with mutant mtDNA dominating in a mosaic manner (Engel and Cunningham, 1963; Hasegawa et al., 1991; Lightowlers et al., 1997).

Muscle sections from a normal subject and patients with CPEO or MELAS were stained for activity of SDH and cytochrome c oxidase (COX) and with anti-MIDAS antibody. No MIDAS-positive fibers were detected in normal muscle, whereas MIDAS-positive fibers were detected in the muscle sections of affected patients (Fig. 2). The amount of MIDAS in the positive muscles increased approximately twofold compared to those in the negative muscles. It is noted that MIDAS was more abundant specifically in fibers with an SDH^{++}/COX^{-} phenotype (Fig. 2, asterisks). Thus, MIDAS is expressed in response to mitochondrial dysfunction in muscle with mitochondrial diseases.

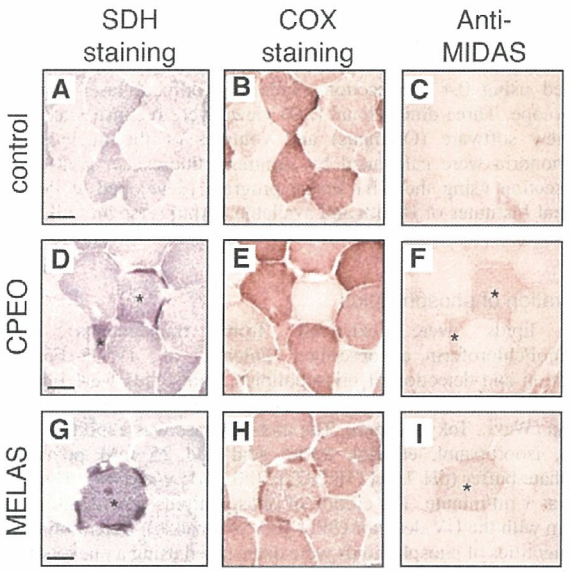

Fig. 2. Expression of MIDAS/GPP34 in SDH^{++}/COX^{-} muscle cells of patients with mitochondrial diseases. Biopsy samples were obtained from the biceps brachii muscle. Activities of SDH and COX were visualized histochemically and the expression of MIDAS/GPP34 was detected with anti-MIDAS antibody. (A-C) Control muscle without mitochondrial disorder. (D-F) Muscle from a patient with CPEO who has a common deletion in mtDNA. (G-I) Muscle from a patient with MELAS who has a point mutation at nucleotide number 3243 in the $tRNA^{Leu(UUR)}$ gene. Asterisks indicate SDH^{++}/COX^{-} cells of patients with increased MIDAS/GPP34 expression. Bars, 50 μm.

Subcellular distribution of MIDAS/GPP34

GPP34 has been isolated as a Golgi peripheral membrane protein in a Golgi proteomics study (Bell et al., 2001). To verify the distribution of MIDAS in mitochondria, we immunostained HeLa cells with an affinity-purified polyclonal antibody against the MIDAS protein. Immunostaining of HeLa cells revealed that MIDAS mainly colocalized with MitoTracker Red (Fig. 3A). The mitochondrial localization was confirmed with another mitochondrial marker, Hsp60 (data not shown). With careful observation, we found MIDAS in an additional region, the perinuclear area, where MitoTracker Red was absent (Fig. 3A, merge; indicated by white arrowhead). This region corresponds to the Golgi apparatus, as judged by immunostaining with anti-p230 (the *trans*-Golgi membrane protein) (Erlich et al., 1996) antibody (Fig. 3B). These results suggest that a majority of MIDAS/GPP34 localizes to mitochondria, but some is distributed in the Golgi apparatus.

This finding disagrees with the previous study on GPP34 showing that GPP34 is located in the Golgi apparatus, but not in mitochondria (Bell et al., 2001). This discrepancy could be due to a different fixation method prior to staining. In general, for immunostaining of cultured cells, the permeabilization of intramembranes with an organic solvent or detergent is essential for antibodies to penetrate the membranes of organelles (Zeller, 1998). In fact, under the same conditions as the published experiment (no permeabilization pretreatment), MIDAS did not show colocalization with mitochondria (Fig. 3D), being detected only in the Golgi apparatus (Fig. 3E). Moreover, several marker proteins were immunostained to confirm that the permeabilization pretreatment with acetate in cold ethanol is essential for detecting the mitochondrial proteins located internally. Without permeabilization pretreatment, cytosolic (Hsc70), mitochondrial outer membrane (Tom20) and *trans*-Golgi (p230) proteins were stained with each antibody (Fig. 3F), whereas the mitochondrial intermembrane space protein (cytochrome c) could not be detected (Fig. 3F). Alternatively, cytochrome c required an acetate/ethanol pretreatment for permeabilization as described in Materials and Methods to be detected (Fig. 3C). Moreover, a mitochondrial matrix protein (Hsp60) and an inner membrane protein (SDH70) were clearly stained only with the acetate/ethanol pretreatment (supplementary material Fig. S3). Therefore, the mitochondrial MIDAS/GPP34 protein is located inside mitochondria or embedded in the outer membrane. In addition, immunostaining with anti-KDEL, the signal peptide targeting the endoplasmic reticulum (ER) (Munro and Pelham, 1987), showed no localization of MIDAS/GPP34 to the ER (data not shown).

To further investigate the subcellular distribution of MIDAS, Myc-tagged constructs were generated. A gene corresponding to a Myc peptide was fused to the gene of the N-terminus (Myc-MIDAS) or C-terminus (MIDAS-Myc) of MIDAS. Fusion constructs were transfected into HeLa cells and the cells were allowed to express the protein for 16 hours. The transfected cells were immunostained with anti-Myc antibody. Myc-MIDAS was localized to the perinuclear area and colocalized with the p230 *trans*-Golgi (Fig. 3G). On the other hand, MIDAS-Myc was distributed in both mitochondria and Golgi as stained with anti-MIDAS antibody (Fig. 3H). This

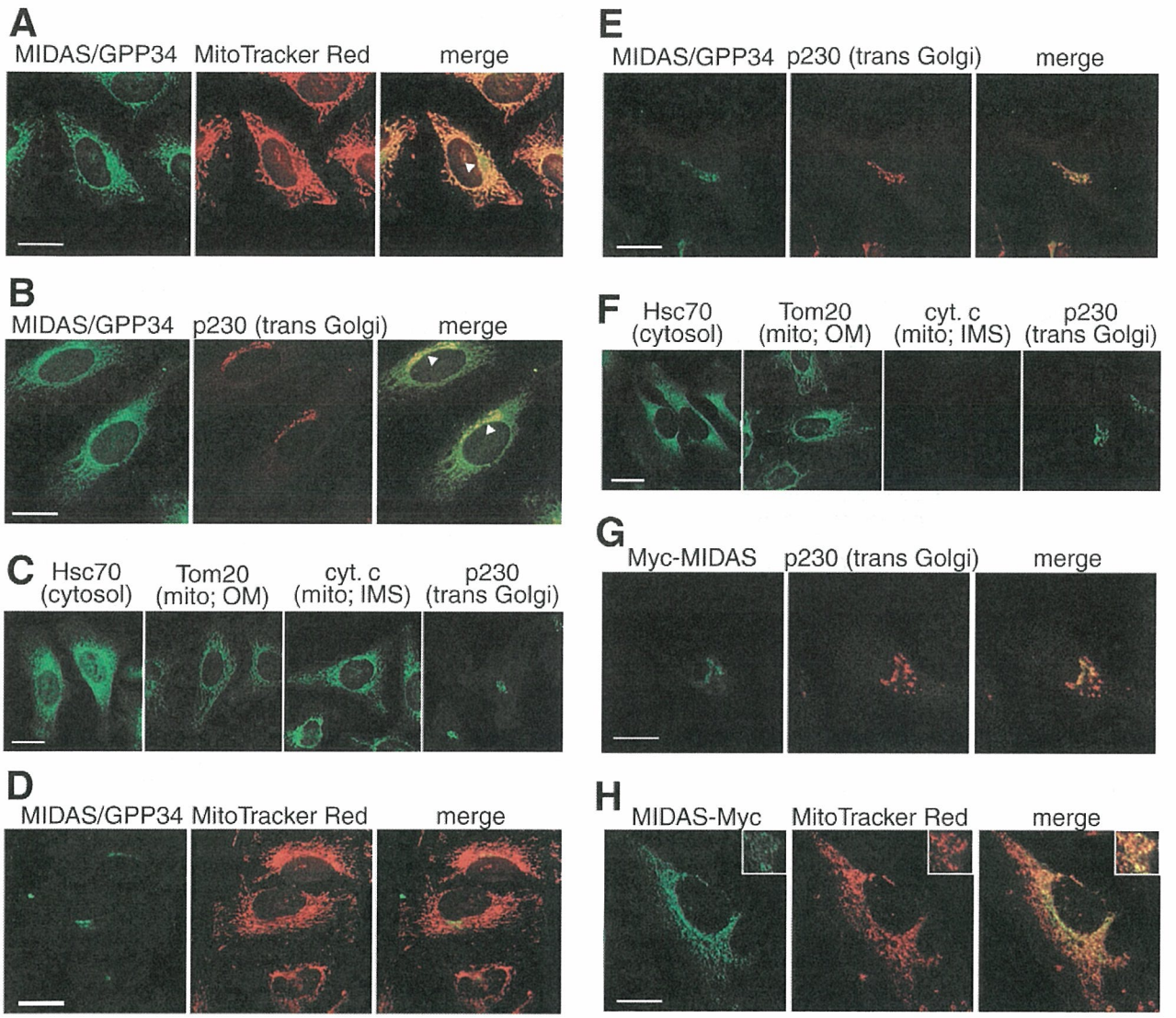

Fig. 3. Localization of MIDAS/GPP34 in mitochondria and the Golgi apparatus. (A-C) HeLa cells in culture were fixed, permeabilized with 5% acetic acid in ethanol and then immunostained with various antibodies. (A) MitoTracker Red (100 nM) was added as a mitochondrial indicator prior to fixation. MIDAS/GPP34 was detected with anti-MIDAS antibody. Arrowhead indicates where MIDAS/GPP34 is more abundant than mitochondria in a perinuclear area. (B) MIDAS/GPP34 and p230 (*trans*-Golgi) were double-stained immunochemically using different secondary antibodies. Arrowheads indicate where the perinuclear area was co-stained with both antibodies. (C) Hsc70 (cytosol), Tom20 (outer membrane of mitochondria), cytochrome c (cyt. c) (intermembrane space of mitochondria) and p230 (*trans*-Golgi) were detected with their respective antibodies. (D-F) HeLa cells in culture were fixed with 4% paraformaldehyde and 4% sucrose without treatment for permeabilization and immunostained with the same procedure as in (A-C). (G,H) Localization of Myc-tagged MIDAS. A Myc tag was fused to the N-terminus (G) or C-terminus (H) of MIDAS. Fusion constructs were transfected into HeLa cells and cells were allowed to express protein for 16 hours. Cells were stained with anti-Myc, anti-p230 antibodies or MitoTracker Red with the same procedure as in (A-C). Bars, 20 μm.

finding suggests that MIDAS potentially localizes to both mitochondria and the Golgi apparatus.

To demonstrate the subcellular distribution of MIDAS, organelles were sub-fractionated with a Nycodenz gradient. HeLa cells were homogenized, the homogenate was fractionated with a 7-35% density gradient and the distribution of MIDAS was examined by western blotting (Fig. 4A). The majority of MIDAS was detected in the mitochondrial fractions (with Tom20 and Hsp60) and small portions were fractionated with the Golgi (with a Golgi marker, Syntaxin6) and cytosol. Relative amounts of MIDAS distributed in the fractions for mitochondria (fractions 13-17), Golgi (fractions 6-12) and cytosol (fractions 1-5) were 0.75, 0.19 and 0.06, respectively, as judged by the densities of total bands.

To determine the sub-mitochondrial distribution of MIDAS, the mitochondria purified from HeLa cells were treated with

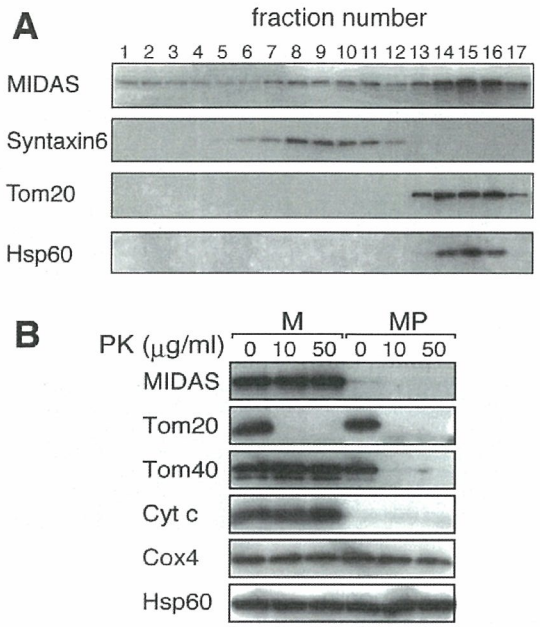

Fig. 4. Localization of MIDAS/GPP34 in the mitochondrial intermembrane space. (A) Fractionation of organelles of HeLa cells in 7-35% (w/v) preformed density gradients. The distribution of MIDAS was detected by western blotting. Syntaxin6 was used for a Golgi marker. Tom20 and Hsp60 were used for mitochondrial markers. (B) Mitoplasts were obtained from the mitochondrial fraction (fraction 15 in A) by osmotic disruption of the outer membrane. The mitochondria (M; lanes 1-3) and the mitoplasts (MP; lanes 4-6) were treated with proteinase K (PK; 10 μg/ml or 50 μg/ml). Mitochondrial sub-fractions were monitored by western blotting with antibodies directed against Tom20 (an outer membrane protein; most of which is exposed outside mitochondria), Tom40 (an outer membrane protein), cytochrome c (cyt c) (an intermembrane space protein), Cox4 (an inner membrane protein) and Hsp60 (a matrix space protein).

proteinase K. Both Tom40 and Tom20 are embedded in the outer membrane, whereas Tom20 is exposed to the outside of mitochondria (Pfanner and Geissler, 2001). Tom20 was easily digested with 10 μg/ml proteinase K, whereas Tom40 and MIDAS were resistant (Fig. 4B, M). On the other hand, when mitochondria were converted to mitoplasts, MIDAS disappeared (Fig. 4B, MP) even without proteinase K, as cytochrome c disappeared. From these results, it was concluded that the majority of MIDAS protein is located in the intermembrane space of mitochondria, with a small fraction present in the Golgi apparatus.

Mitochondrial accumulation without swelling by MIDAS

To determine the function of MIDAS in mitochondria, HeLa cells were transfected with *MIDAS* cDNA under the control of the CMV promoter. We could isolate transfectants constitutively expressing MIDAS at low levels (1.5- to 2-fold increase) (Fig. 5A, upper left panel, CMV-MIDAS3 and CMV-MIDAS9). Cells transiently transfected with a higher level of MIDAS could undergo cell division once or twice but did not survive for a week (data not shown), suggesting that overproduction of MIDAS prevents cell growth. To downregulate MIDAS, we then constructed HeLa transfectants expressing siRNA (small interfering RNA) of *MIDAS* to inhibit the endogenous MIDAS expression (Fig. 5A, upper right panel).

These transfectants were stained with MitoTracker Red to visualize mitochondria, in a short period to monitor the membrane potential of mitochondria. Even low levels of additional MIDAS expression caused a change in the distribution of mitochondria. The mitochondria in a *MIDAS* transfectant CMV-MIDAS3 were concentrated around the nucleus (Fig. 5B, second panel), whereas those in the control transfectants remained dispersed (Fig. 5B, first panel).

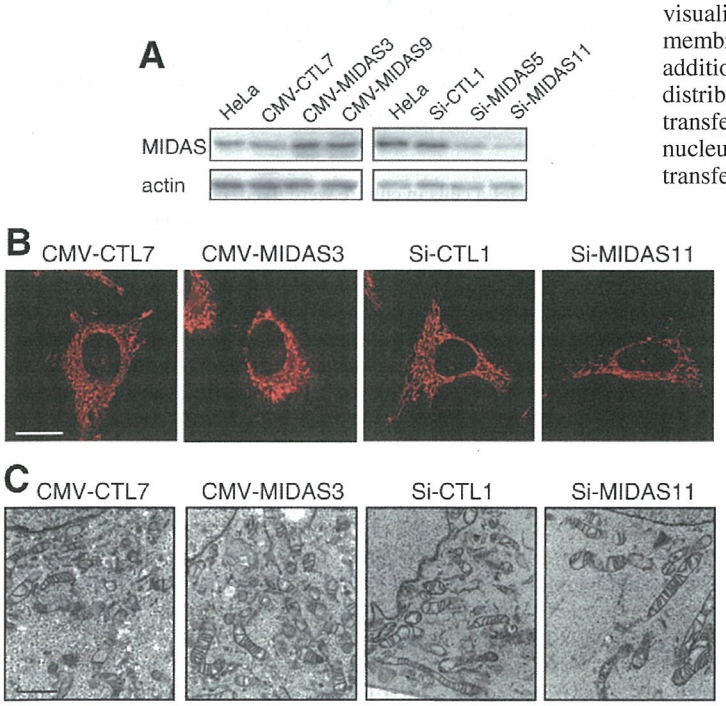

Fig. 5. The increased or decreased mass of intact mitochondria related to MIDAS concentration. (A) CMV-CTL7 and Si-CTL1 are stable control transfectants derived from HeLa cells. Although CMV-MIDAS3 and CMV-MIDAS9 are stable *MIDAS* transfectants under the control of the CMV promoter. Si-MIDAS5 and Si-MIDAS11 were transfectants expressing siRNA of *MIDAS* constitutively. Total cell lysate was extracted from each transfectant cell line and subjected to western blotting with anti-MIDAS and anti-actin antibodies. (B) Control (CMV-CTL7 and Si-CTL1), *MIDAS* transfectants (CMV-MIDAS3) and siRNA *MIDAS* transfectants (Si-MIDAS11) were stained with MitoTracker Red and visualized by confocal scanning laser microscopy. (C) Electron micrographs (×8000) of mitochondria in the transfectants. Bar, 20 μm (B); 1 μm (C).

Moreover, mitochondria in the MIDAS-expressing transfectants were stained more strongly than those in the control cells. Another transfectant clone CMV-MIDAS9 showed the same results (data not shown).

The mitochondria in a siRNA *MIDAS* transfectant, Si-MIDAS11, were dispersed similarly to those in the control transfectant (Si-CTL1) but were less intensely stained (Fig. 5B, third and fourth panels). Another siRNA *MIDAS* transfectant, clone Si-MIDAS5, showed the same results (data not shown).

Electron microscopy showed that mitochondria in the *MIDAS* transfectant were somewhat larger with no marked change in morphology and were neither pathologically swollen nor had lost the cristae structure (Fig. 5C, second panel). In addition, the *MIDAS* transfectants increased the number of mitochondria, whereas the siRNA-transfectants decreased the number of mitochondria (Fig. 5C, fourth panel). These photographs suggest that the number of mitochondria around the nucleus was increased by MIDAS.

Increase in total mitochondrial mass by MIDAS

To quantify the accumulation of mitochondria suggested above, cells were stained with two mitochondria-specific dyes, MitoTracker Red and MitoTracker Green and subjected to flow cytometric analysis (Fig. 6A-C). There was no significant difference in forward scatter among any of the cells examined (FS in Fig. 6C), indicating that MIDAS does not have any influence on cell size, regardless of the up- or downregulation of its expression. MitoTracker Green, but not MitoTracker Red, binds to mitochondria in a membrane-potential-independent manner and fluoresces only in the lipid environment of mitochondria. Fluorescent intensity in green (MitoTracker Green) was measured to estimate overall mitochondrial mass, whereas fluorescent intensity in red (MitoTracker Red) was measured to assess the content of energized mitochondria. The intensities in green and red significantly increased in MIDAS-expressing transfectants (CMV-MIDAS) (Fig. 6A,C). On the other hand, the green and red intensities decreased in the MIDAS downregulated transfectants (Si-MIDAS) (Fig. 6B,C). Quantitative analysis showed that the fluorescent intensities increased 1.5- to 2-fold in the MIDAS-expressing transfectants and decreased to 60-70% in the downregulated transfectants, compared to the control cells, respectively (Fig. 6C). The ratio of the intensity in red to the intensity in green was the same in all the cells examined, indicating that MIDAS does not exert any influence on the membrane potential. To confirm the increase in mitochondria, we stained transfectants with an additional fluorescent dye, TMRM (tetra-methyl-rhodamine methyl ester) specific to mitochondria and obtained a consistent result (supplementary material Fig. S4).

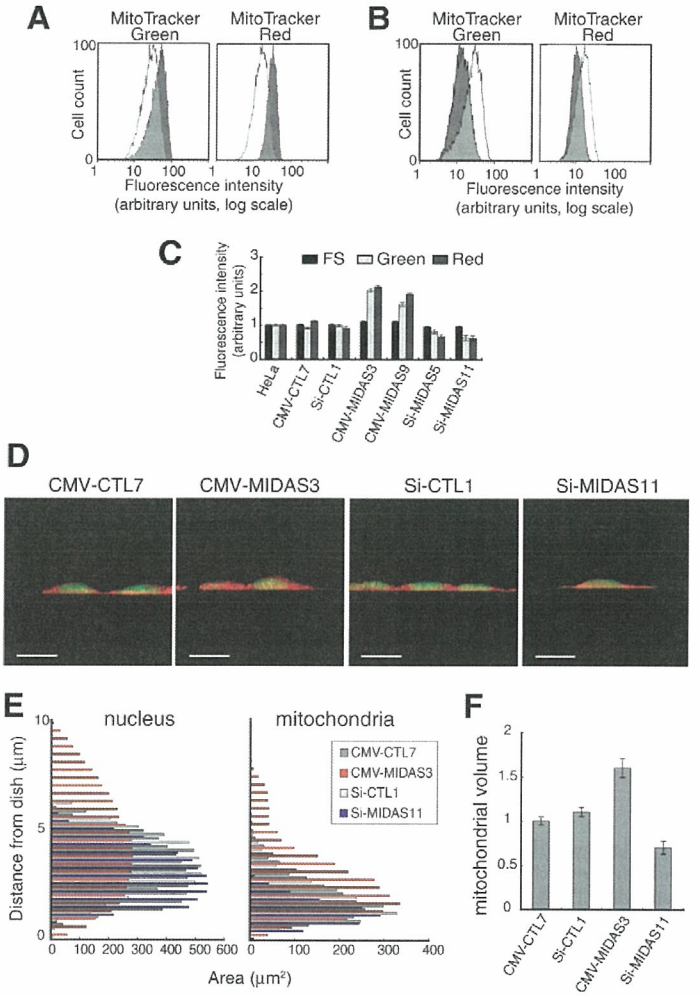

Fig. 6. Changes in mitochondrial mass with MIDAS. (A) Flow cytometric profiles of the fluorescence of dyes specific to mitochondria in CMV-CTL7 (white) and CMV-MIDAS3 (gray). Living transfectants were stained with MitoTracker Green (left) or MitoTracker Red (right) and analyzed with a flow cytometer. (B) Flow cytometric analysis performed with Si-CTL1 (white) and Si-MIDAS11 (gray) cells as described in A. (C) Fluorescence intensity (MitoTracker Green and MitoTracker Red) as well as forward scatter (FS) of HeLa cells and transfectants as quantified by flow cytometry. Values are the mean±s.d. (D) The mitochondria and nucleus in control transfectants (CMV-CTL7 and Si-CTL1), *MIDAS* transfectants (CMV-MIDAS3) and siRNA *MIDAS* transfectants (Si-MIDAS11) were stained with MitoTracker Red and SYTO 16 (green), respectively and scanned by confocal laser microscopy in each 0.4 μm section. Then the side view of a three-dimensional image was reconstructed with Fluoview software. (E) Areas of the nucleus and mitochondria were measured for each section. (F) The total mass of mitochondria in the transfectants was calculated based on the values in E and normalized to that of nucleus. Data represent the mean±s.d. of three sets of experiments. Bars, 20 μm.

The increase in the fluorescence of MitoTracker Green strongly suggests a substantial increase in total mitochondrial mass caused by MIDAS. Therefore, we estimated total mitochondrial volume by three-dimensional reconstitution of cells. Cells were stained with MitoTracker Red (red) for mitochondria and SYTO 16 (green) for the nucleus, respectively. The cells were scanned from bottom to top at intervals of 0.4 μm and each image was analyzed to measure the areas stained with MitoTraker Red and SYTO 16,

separately (Fig. 6E). Interestingly, the side view of the reconstituted three-dimensional image showed that mitochondria in the transfectants expressing MIDAS accumulated at the periphery of the nucleus (Fig. 6D, second panel), whereas in the downregulated transfectants, mitochondria appeared to be decreased in number (Fig. 6D, fourth panel). It is noted that there was no difference in nuclear volume between cells, although their three-dimensional shapes were different. On average, mitochondria occupied 22%, 35% and 15% of the total cytoplasm in controls, MIDAS-expressing transfectants and siRNA transfectants, respectively. The total volume of mitochondria was increased 1.6-fold by the MIDAS expression and decreased 0.75-fold by the downregulation of MIDAS, when normalized to that of the nucleus (Fig. 6F). Thus, the total mitochondrial mass varied more than 2.3-fold with the up- and downregulation of MIDAS. These results clearly indicate that MIDAS regulates total mitochondrial mass.

Regulation of cardiolipin by MIDAS

Flow cytometric analysis using MitoTracker Green showed that mitochondrial lipids varied in a MIDAS-dependent manner. Furthermore, the analysis using the fluorescent dye NAO (nonyl acridine orange), which detects cardiolipin, a mitochondria-specific phospholipid, revealed that the amount of cardiolipin varied according to amount of MIDAS (supplementary material Fig. S5). To obtain direct evidence for an increase in mitochondrial lipids caused by MIDAS, we measured levels of cardiolipin by HPLC. Total lipids were extracted from each transfectant and separated by HPLC as described in the Materials and Methods (Fig. 7A). The peak of cardiolipin (CL) was found to increase in MIDAS-expressing transfectants, compared with control transfectants. In clear contrast, the CL peak decreased in the MIDAS downregulated transfectants. The relative amount of each phospholipid was quantified based on the HPLC peak (Fig. 7B). The results showed that the amount of cardiolipin was increased 1.75-fold in the MIDAS-expressing transfectant and decreased 0.65-fold in the downregulated transfectant, when normalized to that of phosphatidylcholine. Thus, the amount of cardiolipin varied more than 2.6-fold with the up- and downregulation of MIDAS.

Mitochondrial DNA, RNA and proteins were not affected by MIDAS

To understand the mitochondrial increase induced by MIDAS, we examined other mitochondrial components, mitochondrial DNA, RNA and proteins (Fig. 7C). The amount of mtDNA was analyzed by Southern blotting and no significant change was observed. Northern blotting also revealed no change in the stationary amounts of COX II mRNA transcribed from mtDNA. Immunoblots revealed no increase in mitochondrion-

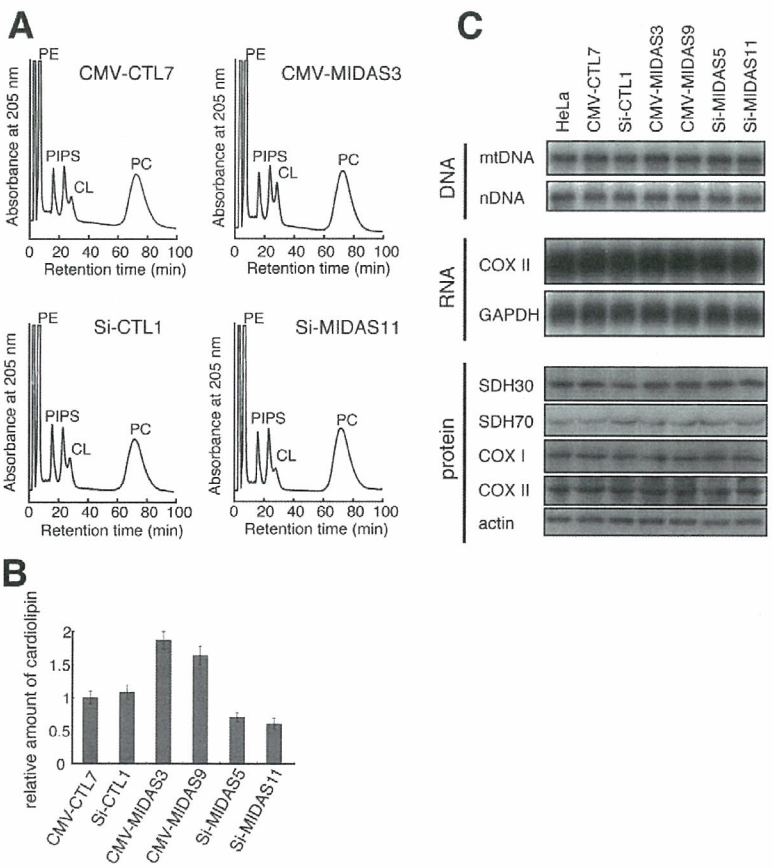

Fig. 7. Effects of MIDAS on amounts of cardiolipin (a mitochondria-specific lipid), mitochondrial DNA, RNA and proteins. (A) Total lipids were extracted from control transfectants (CMV-CTL7 and Si-CTL1), *MIDAS* transfectants (CMV-MIDAS3) and siRNA *MIDAS* transfectants (Si-MIDAS11) and fractionated by HPLC as described in the Materials and Methods. The elution of phospholipids was monitored at 205 nm. CL, cardiolipin; PC, phosphatidylcholine; PE, phosphatidylethanolamine; PI, phosphatidylinositol; PS, phosphatidylserine. (B) The amount of cardiolipin in the transfectants was quantified based on the values in A and normalized to that of phosphatidylcholine. Mean values for three sets of experiments are shown with the s.d. (C) The amount of DNA in HeLa cells and transfectants was analyzed by Southern blotting. To detect mtDNA we used the COX II region in mtDNA as a probe. The nDNA (nuclear DNA) was a loading control and the 18S ribosomal DNA region was used as a probe. The expression of mtDNA and nDNA was analyzed by northern blotting. Blots of total RNA extracted from HeLa and transfectants were hybridized with *COX II*- and *GAPDH* -specific probes. Proteins were analyzed by western blotting. SDH30 and SDH70 are the nucleus-encoded 30 kDa and 70 kDa subunit of SDH, respectively. COX I and COX II are the mitochondrial DNA-encoded subunits.

encoded proteins, COX I and COX II and nucleus-encoded mitochondrial proteins, the 30 kDa and 70 kDa subunits of SDH.

Discussion

In this study, we found three nuclear genes that respond to the depletion of mtDNA. Although mtDNA was completely depleted after a long exposure of HeLa cells to ethidium bromide, its nuclear genes may be affected at a high frequency. Thus, we used a cybrid clone, Ft2-11, that had been obtained by the intercellular transfer of wild-type mitochondria into EB8 cells as a control instead of parental HeLa cells. This procedure, cell fusion between enucleated cells (mitochondrion donor) and EB8 cells, would cause no damage to the nuclear genes.

On comparing the mRNA isolated from EB8 cells with that of control cells by differential display, we found three genes whose expression was higher in EB8 cells. Two of them were the apurinic/apyrimidinic endonuclease I (APE1/HAP1) (Demple et al., 1991) and DNA ligase III genes (Wei et al., 1995). These gene products are located in mitochondria as well as the nucleus and are involved in DNA repair. Thus, it is reasonable to assume that the mitochondrial repair system responds to the depletion of mtDNA.

The third gene product, named MIDAS here, was identical to a Golgi protein, GPP34. The nucleotide sequence of *MIDAS/GPP34* is conserved from yeast to human (Bell et al., 2001; Wu et al., 2000). Its yeast *Saccharomyces cerevisiae* homolog (YDR372c) has been deleted revealing that the gene is not essential for viability (Winzeler et al., 1999; Bidlingmaier and Snyder, 2002). Although a mutation in the YDR372c gene revealed a phenotype with an abnormal budding (Bidlingmaier and Snyder, 2002) and aberrant in protein-vacuolar targeting (Bonangelino et al., 2002), the molecular function of the gene product remains unknown. Genetic analysis showed that there are genetic interactions between YDR372c and intracellular protein-transport factors (RIC1 and YPT6) (Tong et al., 2004). As MIDAS has a leucine-zipper motif (supplementary material Fig. S1), it may interact with a protein involved in intracellular protein transport through this motif.

In most mitochondrial diseases, mutant mtDNA coexists with wild-type mtDNA at various ratios in a heteroplasmic manner and exhibits a cognate pathological phenotype in a threshold-dependent manner. COX-deficient cells have abundant mutant mtDNA, whereas COX-positive cells have a small amount of mutant mtDNA. MIDAS was shown to be more abundant in muscle cells with no COX activity in patients with mitochondrial diseases. This finding indicates that the enhanced expression of MIDAS occurs not only in HeLa cells lacking mtDNA, but also in muscle cells with pathogenic mutant mtDNAs, regardless of point mutations or deletions of mtDNA. MIDAS has putative ATF-1 binding sites and the upregulated expression by EWS/ATF-1 chimeric transcription factor was revealed (Jishage et al., 2003). When mitochondrial dysfunction occurs, the expression of MIDAS may be activated by CREB/ATF-1 family transcription factors.

A previous report (Bell et al., 2001) indicated that GPP34 colocalizes only with Golgi, but not mitochondria. When we used the method they described (Bell et al., 2001) with permeabilization pretreatment after fixation, anti-MIDAS antibody stained only the Golgi apparatus (Fig. 3D,E). On the other hand, immunostaining clearly showed that MIDAS colocalized with both mitochondria and the Golgi apparatus when the cells were subjected to the acetate/ethanol pretreatment to permeabilize the mitochondrial membranes. An outer membrane protein (Tom 20) did not require the permeabilization procedure for staining, but the acetate/ethanol procedure was essential for the proteins located inside mitochondria such as cytochrome c, Hsp60 and SDH70 (Fig. 3C and supplementary material Fig. S3). Thus, the discrepancy is fully explained by the difference in the permeabilization method used (Fig. 3). The present result is consistent with the result of a sub-organellar fractionation experiment that showed that MIDAS is present in the intermembrane space. Thus, it is concluded that the antibody against MIDAS/GPP34 cannot access the mitochondrial MIDAS without the permeabilization pretreatment. As MIDAS lacks typical sequences that could target mitochondria or the Golgi apparatus, it is unknown how it is directed to the respective organelle.

As MIDAS/GPP34 has an isoform, named GPP34R, one may target mitochondria and the other may target the Golgi apparatus. However, this is unlikely because GPP34R was expressed at a level less than 2% of that of MIDAS in HeLa cells. This small amount cannot account for the relative amount of the protein located in the Golgi apparatus. In addition, we performed a crucial experiment. As the fusion protein comprising Myc-tag and the N-terminus of MIDAS targets only Golgi, the N-terminal region may be responsible for targeting mitochondria. In contrast, an alternative fusion protein with Myc-tag at the C-terminus of MIDAS targets mitochondria. This experiment suggests that the single molecule has the potential to localize to two distinct organelles. Further experiments will reveal which location of MIDAS contributes to its distribution.

Mitochondria gathered around the nucleus in MIDAS-expressing transfectants. As mitochondria often gather around the nucleus in sick cells regardless of internal or external conditions, it may be that toxicity of MIDAS forces mitochondria to concentrate around the nucleus by affecting the cytoskeletal structure. However, no abnormal cytoskeletal structure was found in MIDAS-expressing transfectants (supplementary material Fig. S6). Thus, the mitochondrial accumulation was not due to abnormality of the cytoskeleton. The mitochondrial biogenesis occurs near the nucleus and fresh mitochondria are transported to peripheral areas (Yaffe, 1999). Thus, newly synthesized mitochondria seem to be concentrated around the nucleus and then the excess mitochondria may push up the nucleus as seen in Fig. 5B and Fig. 6D, second panel.

A transcriptional coactivator PGC-1 enhances the expression of many mitochondrial proteins by activating several transcription factors, such as NRF-1, NRF-2, Sp1, YY1, CREB and MEF-2/E-box (Scarpulla, 2002). Recognition sites for NRF-1, NRF-2 and Sp1 are common to most nuclear genes encoding components involved in mitochondrial respiration, transcription and replication (Scarpulla, 2002). However, it is unknown how PGC-1 contributes to the increase in mitochondrial lipids. In addition, there has been no report that PGC-1 is expressed in response to mitochondrial dysfunction or damage. MIDAS seems to accumulate mitochondria by an

Journal of Cell Science